J. Fluid Mech. (2011), *vol.* 669, *pp.* 120–166. © Cambridge University Press 2011
doi:10.1017/S0022112010004933

Lagrangian blocking in highly viscous shear flows past a sphere

ROBERTO CAMASSA, RICHARD M. McLAUGHLIN AND LONGHUA ZHAO†

Department of Mathematics, University of North Carolina at Chapel Hill, NC 27599, USA

(Received 6 April 2010; revised 17 September 2010; accepted 20 September 2010)

An analytical and computational study of Lagrangian trajectories for linear shear flow past a sphere or spheroid at low Reynolds numbers is presented. Using the exact solutions available for the fluid flow in this geometry, we discover and analyse blocking phenomena, local bifurcation structures and their influence on dynamical effects arising in the fluid particle paths. In particular, building on the work by Chwang & Wu, who established an intriguing blocking phenomenon in two-dimensional flows, whereby a cylinder placed in a linear shear prevents an unbounded region of upstream fluid from passing the body, we show that a similar blocking exists in three-dimensional flows. For the special case when the sphere is centred on the zero-velocity plane of the background shear, the separatrix streamline surfaces which bound the blocked region are computable in closed form by quadrature. This allows estimation of the cross-sectional area of the blocked flow showing how the area transitions from finite to infinite values, depending on the cross-section location relative to the body. When the sphere is off-centre, the quadrature appears to be unavailable due to the broken up-down mirror symmetry. In this case, computations provide evidence for the persistence of the blocking region. Furthermore, we document a complex bifurcation structure in the particle trajectories as the sphere centre is moved from the zero-velocity plane of the background flow. We compute analytically the emergence of different fixed points in the flow and characterize the global streamline topology associated with these fixed points, which includes the emergence of a three-dimensional bounded eddy. Similar results for the case of spheroids are considered in Appendix B. Additionally, the broken symmetry offered by a tilted spheroid geometry induces new three-dimensional effects on streamline deflection, which can be viewed as effective positive or negative suction in the horizontal direction orthogonal to the background flow, depending on the tilt orientation. We conclude this study with results on the case of a sphere embedded at a generic position in a rotating background flow, with its own prescribed rotation including fixed and freely rotating. Exact closed-form solutions for fluid particle trajectories are derived.

Key words: bifurcation, low-Reynolds-number flows, particle/fluid flows

1. Introduction

Fluid flow past a rigid body is a fundamental problem in fluid dynamics. It plays an important role in the study of particle entrainment, sediment transport,

† Present address for correspondence: School of Mathematics, University of Minnesota, MN 55455, USA. Email: lzhao@umn.edu

https://doi.org/10.1017/S0022112010004933 Published online by Cambridge University Press

microfluidic mixing, micro-organism locomotion and many other areas of geophysical and biophysical interests. An important class of problems concerns scales where inertia plays a subdominant role to viscous forces, which is the case for many biophysical applications. The Stokes approximation becomes relevant in such cases, despite its limitations in governing fluid motion far from the body. While the case of uniform flows and its ensuing far-field paradoxes in two and three dimensions are well known, features associated with (spatially) non-uniform fluid flows at the far field have received comparatively less attention in the literature.

For far-field linear flows, some experimental and analytical results have been presented by Jeffery (1922), Cox, Zia & Mason (1968), Robertson & Acrivos (1970), Kossack & Acrivos (1974), Poe & Acrivos (1975) and Chwang & Wu (1975). In particular, Jeffery (1922) provided the solutions for both fluid and body motions for the case of an ellipsoid free to move under the fluid–body forces in an imposed far-field linear flow. Even when the velocity field is analytically available, the Lagrangian viewpoint of the fluid particle motion is seldom studied and general solutions are naturally not available. Interestingly, for a freely rotating sphere with its centre fixed at the zero-velocity (say, horizontal) plane of a background linear shear, Cox *et al.* (1968) computed fluid particle trajectories in closed form by quadratures. For a fixed body, there are even fewer results for particle trajectories. Bretherton (1962), and later Chwang & Wu (1975), present an expression for the streamfunction for the two-dimensional flow around a fixed disk with its centre on the zero-velocity line in a linear shear. (We will hereafter use the terminology 'disk' to refer to an infinitely long cylinder whose axis is perpendicular to the background stream, i.e. an inherently two-dimensional set-up). These authors noted an interesting blocking phenomenon which was observed numerically and experimentally by Robertson & Acrivos (1970) and Poe & Acrivos (1975). This blocking behaviour is a strong modification of the particle trajectories from situations without and with a fixed disk: in the absence of the body, particles are swept by the shear flow on straight horizontal lines, never crossing the zero-velocity horizontal line. When the disk is placed into the flow, two regions of fluid emerge in which particles cross the zero-velocity line as they approach the disk in either forward or backward time. Particles initially within these regions are confined to them, and will never pass through the vertical line through the disk's centre orthogonal to the background shear flow. One of the aims of this paper is to analyse this kind of phenomenon in more general three-dimensional flows associated with spheres and spheroids. Such studies may find further application in more complex situations involving the addition of electrostatic interactions such as reviewed by Spielman (1977) and Feke & Schowalter (1983), who reported on aspects of particle trapping and aggregation for situations involving the addition of attractive and repulsive interactive forces.

Generally, the regions where blockage occurs are bounded by separation 'stream-surfaces'. In the two-dimensional case involving a linear shear flow past a disk, the height of these separation streamlines becomes infinite far from the disk, an effect which was observed by Bretherton (1962) and Chwang & Wu (1975) and was conjectured not to persist in a three-dimensional shear flow past a fixed sphere. This case does not appear to have been studied in detail, although particle trajectories are sketched in the symmetry plane by Robertson & Acrivos (1970) and Leal (2007).

Most of the existing literature seems to concentrate on the flow velocity field and the forces acting on the sphere, see for example, Jeffery (1922), Saffman (1965), Chwang & Wu (1975), Pozrikidis (1997), Mikulencak & Morris (2004) and Kim & Karrila (2005).

https://doi.org/10.1017/S0022112010004933 Published online by Cambridge University Press

Here we demonstrate that the blocking phenomenon persists in the three-dimensional flows for the simple linear shear flow past a fixed sphere, and obtain explicit expressions for the blocking regions, such as the bounding stream surfaces and asymptotic estimates for the blocked regions in the far field.

This paper is organized as follows. In § 2, we introduce the problem and the velocity field for an unbounded linear shear flow past a fixed sphere. In § 3, we integrate by quadratures the fluid particle equations when the sphere's centre is in the zero-velocity plane. In particular, we study in detail the stagnation points with their associated surfaces, as these provide the framework for the blocked region geometry, and the mode of divergence of the blocked regions' cross-sectional area is calculated. Section 4 examines the flow field bifurcations as the centre of the sphere is moved off the zero-velocity plane. Numerical results illustrate the global bifurcations and demonstrate the persistence of the blocked regions. In § 5, we consider the case of a rotating sphere embedded in a rotating fluid, which is perhaps more relevant to mixing applications. In Appendix B, we provide results for the case of spheroids. The blocking phenomenon in this case has new features with respect to the spherical case, including deformation of fluid particle trajectories in a positive and negative suction pattern depending on the orientation of the spheroid with respect to the background shear.

2. Formulation of the problem

We study the motion of an unbounded linear shear flow $\boldsymbol{U} = \Omega z \boldsymbol{e}_x + U \boldsymbol{e}_x$ of constant density ρ and dynamic viscosity μ, past a fixed sphere

$$x^2 + y^2 + z^2 = a^2. \tag{2.1}$$

Since the fluid is incompressible, the continuity equation is

$$\operatorname{div} \boldsymbol{u} = 0, \tag{2.2}$$

where $\boldsymbol{u}$ is the fluid velocity. In this paper, we assume that the inertial terms in the Navier–Stokes equations can be neglected. Thus, the equations of motion are

$$\mu \nabla^2 \boldsymbol{u} = \nabla p, \tag{2.3}$$

where p denotes the fluid pressure. The condition for (2.3) to hold is that $Re = \Omega a^2 \rho / \mu \ll 1$. The boundary conditions are that $\boldsymbol{u} = 0$ on the solid boundary, and $\boldsymbol{u}$ is asymptotic to the basic shear flow at large distances from the rigid body.

A schematic diagram of the problems is shown in figure 1. Case 1 in figure 1(a) is the shear flow $\Omega z \boldsymbol{e}_x$ past a fixed sphere at the origin. Case 2 in figure 1(b) is the shear $\Omega z \boldsymbol{e}_x + U \boldsymbol{e}_x$ past the sphere, where the centre of the sphere is out of the zero-velocity plane of the background shear.

The exact velocity field is constructed by employing Stokes doublets associated with the base vectors $\boldsymbol{e}_x$ and $\boldsymbol{e}_y$ and potential quadrupole in Chwang & Wu (1975). More details about fundamental singularities can be found in their paper. The velocity field $\boldsymbol{u}$ for a fixed sphere in the linear shear is

$$\begin{aligned} \boldsymbol{u} = \Omega \left(z \boldsymbol{e}_x - \frac{5a^3}{6} \frac{3xz\boldsymbol{x}}{r^5} + \frac{a^3}{2} \frac{\boldsymbol{e}_y \times \boldsymbol{x}}{r^3} - \frac{a^5}{6} \nabla \frac{\partial^2}{\partial x \partial z} \frac{1}{r} \right) \\ + U \left\{ \boldsymbol{e}_x - \frac{3a}{4} \left[\frac{\boldsymbol{e}_x}{r} + \frac{(\boldsymbol{e}_x \boldsymbol{x}) \boldsymbol{x}}{r^3} \right] + \frac{a^3}{4} \nabla \frac{\partial}{\partial x} \frac{1}{r} \right\}, \end{aligned} \tag{2.4}$$

https://doi.org/10.1017/S0022112010004933 Published online by Cambridge University Press

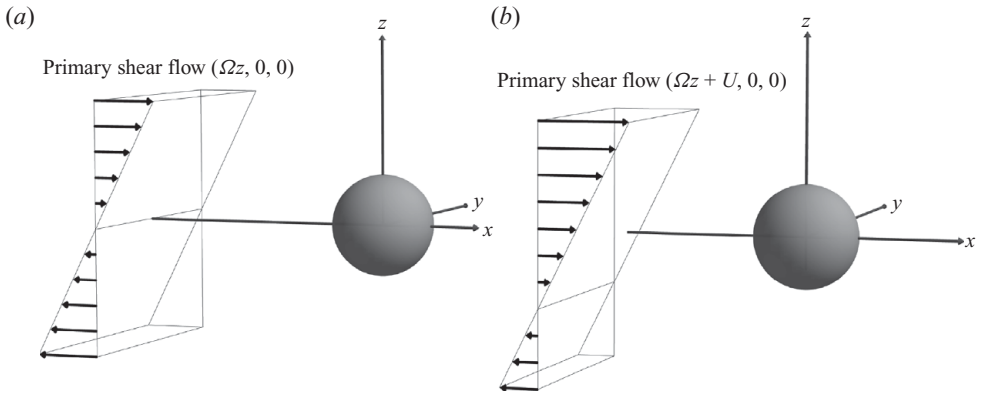


FIGURE 1. Flow past a fixed sphere $x^2+y^2+z^2=a^2$. Without loss of generality, assume $\Omega \geqslant 0$ and $U \geqslant 0$.

where $\boldsymbol{x}=(x, y, z)$, $r=|\boldsymbol{x}|=\sqrt{x^2+y^2+z^2}$, $\boldsymbol{e}_x$, $\boldsymbol{e}_y$ and $\boldsymbol{e}_y$ are the unit vectors along the x, y and z directions, respectively. The force acting on the fixed sphere is $\boldsymbol{F}=6\pi\mu\, U\boldsymbol{e}_x$ and the torque at the origin is $\boldsymbol{T}=-4\pi\mu\, \Omega\, a^3\boldsymbol{e}_z$, as shown by Chwang & Wu (1975).

Let $\boldsymbol{x}'=\boldsymbol{x}/a$, $\boldsymbol{u}'=\boldsymbol{u}/(a\Omega)$ and $U'=U/(a\Omega)$, non-dimensionalizing the equations (dropping the primes), the non-dimensional velocity field is

$$\boldsymbol{u}=z\boldsymbol{e}_x-\frac{5}{2}\frac{xz\boldsymbol{x}}{r^5}+\frac{\boldsymbol{e}_y\times\boldsymbol{x}}{2r^3}-\frac{1}{6}\nabla\frac{\partial^2}{\partial x\partial z}\frac{1}{r} + U\left[\boldsymbol{e}_x-\frac{3}{4}\left(\frac{\boldsymbol{e}_x}{r}+\frac{(\boldsymbol{e}_x\,\boldsymbol{x})\boldsymbol{x}}{r^3}\right)+\frac{1}{4}\nabla\frac{\partial}{\partial x}\frac{1}{r}\right]. \quad (2.5)$$

From now on, we use the non-dimensional variables unless stated otherwise.

3. Shear past a sphere whose centre is in the centreplane

In this section, we first derive closed formulae for the fluid particle trajectories in the case of an unbounded linear shear past a fixed unit sphere, whose centre lies in the zero-velocity plane of the background shear flow. Then, we investigate the blocking phenomenon based on the trajectory equations. We report results on the flow structure on the $y=0$ symmetry plane, followed by results out of this symmetry plane and compare these results with the two-dimensional flow around an infinitely long cylinder. Additionally, we will analytically calculate the stagnation points, the three-dimensional separatrix, and the measurement of blocking regions, and analyse the structure of the flow near the sphere. For this case, the centre of the sphere is in the zero-velocity plane of the background, and the velocity field is a simplified form of (2.5)

$$\boldsymbol{u}=z\boldsymbol{e}_x-\frac{5}{2}\frac{xz\boldsymbol{x}}{r^5}+\frac{\boldsymbol{e}_y\times\boldsymbol{x}}{2r^3}-\frac{1}{6}\nabla\frac{\partial^2}{\partial x\partial z}\frac{1}{r}. \quad (3.1)$$

3.1. *Exact quadrature formulae for the fluid particle trajectories*

Here, streamlines are constructed as the intersection of two stream surfaces for a three-dimensional flow. Of course, it is not always possible to find explicit formulae of streamlines for an arbitrary flow field, and we show how particle trajectories may be computed in closed form for the complex flow studied in this paper.

https://doi.org/10.1017/S0022112010004933 Published online by Cambridge University Press

On the basis of the special geometry of this problem, we change the coordinates from rectangular coordinates to spherical coordinates (r, ϕ, θ). Using the explicit fluid flow, we may immediately write the particle trajectory equations in spherical coordinates as

$$\left.\begin{aligned} \frac{\mathrm{d}r}{\mathrm{d}t} &= \cos\theta \sin(2\phi)\frac{3-5r^2+2r^5}{4r^4}, \\ \frac{\mathrm{d}\theta}{\mathrm{d}t} &= \sin\theta \cot\phi \frac{1+r^2-2r^5}{2r^5}, \\ \frac{\mathrm{d}\phi}{\mathrm{d}t} &= \cos\theta \frac{\cos(2\phi)(r^5-1)+r^5-r^2}{2r^5}, \end{aligned}\right\} \tag{3.2}$$

where $r = \sqrt{x^2+y^2+z^2}$ $(1 \leqslant r < \infty)$, $\phi = \arccos(z/r)$ $(0 \leqslant \phi \leqslant \pi)$ and $\theta = \arctan(y/x)$ $(-\pi \leqslant \theta < \pi)$.

Since ordinary differential equation (ODE) system (3.2) is an autonomous system, we eliminate time t and use the radius r as a new independent variable giving a system for $\mathrm{d}\phi/\mathrm{d}r$ and $\mathrm{d}\theta/\mathrm{d}r$:

$$\frac{\mathrm{d}\theta}{\mathrm{d}r} = \frac{(1+r^2-2r^5)\tan\theta}{(3r-5r^3+2r^6)\sin^2\phi}, \tag{3.3}$$

$$\frac{\mathrm{d}\phi}{\mathrm{d}r} = \frac{-r^2+r^5+(r^5-1)\cos(2\phi)}{r(3-5r^2+2r^5)\cos\phi\sin\phi}. \tag{3.4}$$

Next, changing the variable $y = r\sin\theta\sin\phi$ and taking the derivative of y with respect to r, yields

$$\frac{\mathrm{d}y}{\mathrm{d}r} = \sin\theta\sin\phi + r\cos\theta\sin\phi\frac{\mathrm{d}\theta}{\mathrm{d}r} + r\sin\theta\cos\phi\frac{\mathrm{d}\phi}{\mathrm{d}r}. \tag{3.5}$$

Substituting $\mathrm{d}\theta/\mathrm{d}r$ and $\mathrm{d}\phi/\mathrm{d}r$ into the above equation and replacing $\sin\theta\sin\phi$ with y/r, we get

$$\frac{\mathrm{d}y}{\mathrm{d}r} = \frac{-5(1+r)\sin\theta\sin\phi}{(r-1)(3+6r+4r^2+2r^3)} = \frac{-5(1+r)y}{r(r-1)(3+6r+4r^2+2r^3)}. \tag{3.6}$$

Similarly, take a derivative of $z = r\cos\phi$ with respect to r and substitute $\mathrm{d}\phi/\mathrm{d}r$ into the resulting formula,

$$\frac{\mathrm{d}z}{\mathrm{d}r} = \cos\phi - r\sin\phi\frac{\mathrm{d}\phi}{\mathrm{d}r} = \frac{(1+r)(5\cos^2\phi-1)}{(3+3r-2r^2-2r^3-2r^4)\cos\phi}. \tag{3.7}$$

Replacing $\cos\phi$ with z/r, the above equation becomes

$$\frac{\mathrm{d}z}{\mathrm{d}r} = \frac{(r+1)(r^2-5z^2)}{r(r-1)(3+6r+4r^2+2r^3)z}. \tag{3.8}$$

The obtained ODEs $\mathrm{d}y/\mathrm{d}r$ and $\mathrm{d}z/\mathrm{d}r$ decouple.

Using separation of variables, ODE (3.6) can be solved analytically. The analytic solution is

$$y^3 = C_1\frac{r^5}{(r-1)^2(3+6r+4r^2+2r^3)}. \tag{3.9}$$

https://doi.org/10.1017/S0022112010004933 Published online by Cambridge University Press

The ODE in (3.8) is not exact, and hence not immediately separable; nonetheless, an integrating factor may be found. We rewrite this as

$$\frac{(1+r)(r^2-5z^2)}{(r-1)r(3+6r+4r^2+2r^3)}\,\mathrm{d}r - z\,\mathrm{d}z = 0. \tag{3.10}$$

Notice that multiplying this equation by the integrating factor $(3-5r^2+2r^5)^{2/3}/r^{10/3}$ yields an exact equation which is solved in closed integral form:

$$\int^{1/r} \frac{(1+s)(1-s)^{1/3}}{(2+4s+6s^2+3s^3)^{1/3}}\,\mathrm{d}s - \frac{(3-5r^2+2r^5)^{2/3}}{2\,r^{10/3}}z^2 = C_2. \tag{3.11}$$

Here C_1 and C_2 are constants determined by the initial values y_0, z_0 and $r_0 = \sqrt{x_0^2+y_0^2+z_0^2}$.

Equations (3.9) and (3.11) describe the fluid particle trajectories. If $r_0 \neq 1$, (3.11) can be rewritten as

$$z^2 = \frac{2\,r^{10/3}}{(3-5r^2+2r^5)^{2/3}} \int_{1/r}^{1/r_0} \frac{(1+s)(1-s)}{(2-5s^3+3s^5)^{1/3}}\,\mathrm{d}s + z_0^2 \left(\frac{r}{r_0}\right)^{10/3} \left(\frac{3-5r_0^2+2r_0^5}{3-5r^2+2r^5}\right)^{2/3}. \tag{3.12}$$

This equation expresses the height z of the fluid particle trajectory in terms of r. These trajectory equations provide rigorous tools for studying the blocking phenomenon.

3.2. *Blocking phenomenon*

Here we analyse the blocking phenomenon which occurs in this flow. This blocking behaviour is a strong modification of the particle trajectories from situations without and with a fixed solid sphere present in the flow: In the absence of a solid sphere, particles released in the shear flow (say, starting above the $z=0$ plane) will be swept from large negative x values, to large positive x values as time progresses. However, when the fixed, solid sphere is introduced into the flow, a large measure of particle trajectories lose this streaming property. For example, blocked particles starting with large negative x values do not pass the sphere as time progresses, but rather limit back to large negative x values as time progresses. The regions where this behaviour occurs in three-dimensional space are defined to be the 'blocked regions' of the flow; see figure 2, which depicts this blocked region when the flow is restricted to the two-dimensional symmetry plane. We note that this type of behaviour has been observed for the case of an infinitely long cylinder immersed in a linear shear flow by Chwang & Wu (1975); however, they conjectured that this behaviour would not persist in situations involving a sphere (instead of a cylinder). Here, we show that in fact for the case of the sphere, the blocked region persists and, moreover, we analytically compute the geometry of this region, and show that it has infinite cross-sectional areas. With the exact, closed-form expressions for the particle trajectories given in (3.9) and (3.12), we may proceed directly to compute the geometry of the blocked regions.

3.2.1. *Blocking phenomenon in the $y=0$ symmetry plane*

In the $y=0$ plane, the velocity field is

$$u(x,0,z) = z\left(1 - \frac{1}{2r^3} - \frac{5x^2}{2r^5} - \frac{z^2-4x^2}{2r^7}\right), \tag{3.13}$$

https://doi.org/10.1017/S0022112010004933 Published online by Cambridge University Press

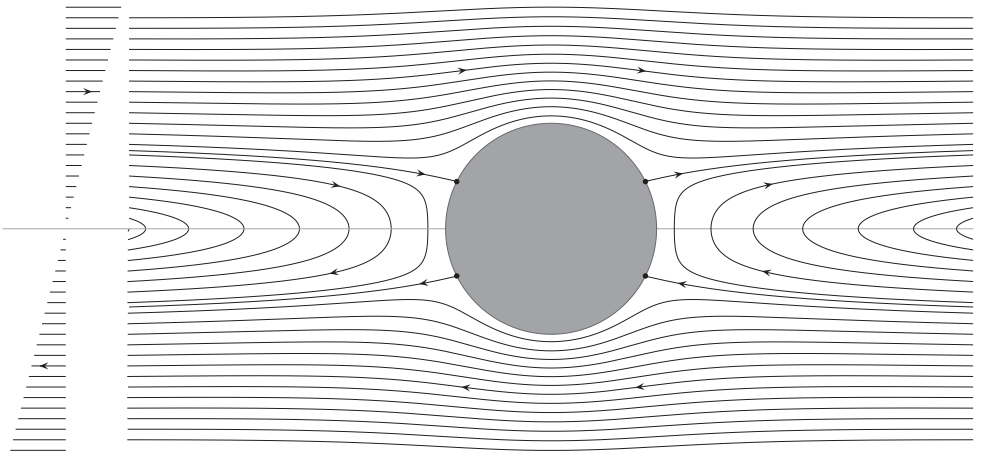


FIGURE 2. Streamlines in the $y=0$ plane with the linear shear flow $z\boldsymbol{e}_x$ past a fixed sphere. The four points mark the stagnation points on the unit sphere in this symmetry plane. Note that the separatrix height limits to approximately 0.88207 and is rigorously less than unity.

$$v(x,0,z)=0, \tag{3.14}$$

$$w(x,0,z)=x\left(\frac{1}{2r^3}-\frac{5z^2}{2r^5}-\frac{x^2-4z^2}{2r^7}\right), \tag{3.15}$$

and $r=\sqrt{x^2+y^2+z^2}=\sqrt{x^2+z^2}$. Notice that one velocity component v vanishes. Particles initially on this plane never leave this plane, i.e. $y=0$ for the particle trajectory. Fluid particles in this plane are thus described by the closed integral formula (3.12) with $r_0^2=x_0^2+z_0^2$ and $r^2=x^2+z^2$. The streamlines in the $y=0$ symmetry plane shown in figure 2 explicitly depict the blocked region. The fully three-dimensional structure of the blocking region will be described below.

The four dots on the sphere in figure 2 are stagnation points, $(x,y,z)=(\pm 2/\sqrt{5},0,\pm 1/\sqrt{5})$ in rectangular coordinates. Two other stagnation points on the sphere are located at $(0,\pm 1,0)$, which are out of this symmetry plane. Stagnation points are special among the fixed points that comprise a no-slip boundary. We define a point on such boundaries to be stagnation points if, for any neighbourhood of one such point, there exists a subset of material fluid points of the neighbourhood that never leave the neighbourhood in backward (for a repelling stagnation point) or forward (for an attracting stagnation point) infinite time.

From figure 2, it is clear that there are blocked regions. For example, the flow is separated by the stagnation line in the second quadrant. Below that stagnation line the flow is trapped on the left side of the sphere.

It is worth comparing this case with that of the analogous two-dimensional flow. For the two-dimensional flow in the case of an infinitely long cylinder immersed in a linear shear flow with the cylinder axis perpendicular to the lines of constant shear, the stream function is

$$\phi(x,z)=\frac{1}{2}z^2\left(1-\frac{1}{r^2}\right)^2+\frac{1}{4}\left(1-\frac{1}{r^2}\right)-\frac{1}{2}\log r, \tag{3.16}$$

see Chwang & Wu (1975) and Jeffrey & Sherwood (1980) for more details. Here $r^2=x^2+z^2$, and the radius of the cylinder is unity. The stagnation points on the cylinder are $(\pm\sqrt{3}/2,\pm 1/2)$. Notice that the separatrix is totally explicit in this case.

https://doi.org/10.1017/S0022112010004933 Published online by Cambridge University Press

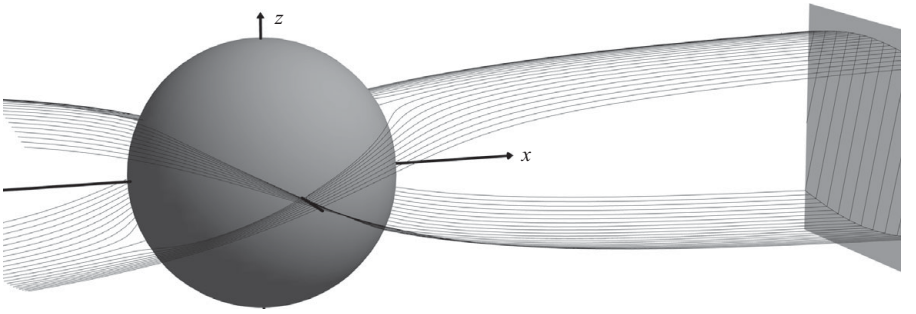


FIGURE 3. Separation surfaces generated by separatrix lines in the flow.

Moreover, as $x \to \pm\infty$, the height $|z|$ of separatrix goes to ∞. This peculiar behaviour is in some sense similar to the well-known Stokes paradox in a two-dimensional uniform flow past a cylinder. Our results below show that the limiting height of the separatrix is finite in the case involving a fixed, rigid sphere, in sharp contrast with the two-dimensional case.

3.2.2. *Blocking phenomenon off the $y=0$ plane*

By continuity, it is expected that the blocking phenomenon extends outside the $y=0$ symmetry plane. Our analytic results not only show the existence of this three-dimensional blocking region but also establish that the height of the blocking region is bounded by a constant less than the sphere radius, and dependent upon the distance off the symmetry plane. (We will compute explicitly the three-dimensional geometry of the blocked region in §§ 3.4 and 3.5.)

Recall (3.9) and (3.12) with the initial value (x_0, y_0, z_0):

$$y = y_0 \frac{r^{5/3}(r_0-1)^{2/3}\left(3+6r_0+4r_0^2+2r_0^3\right)^{1/3}}{r_0^{5/3}(r-1)^{2/3}\left(3+6r+4r^2+2r^3\right)^{1/3}}, \tag{3.17}$$

$$z^2 = \frac{2\,r^{10/3}}{(3-5r^2+2r^5)^{2/3}}\int_{1/r}^{1/r_0}\frac{(1+s)(1-s)^{1/3}}{(2+4s+6s^2+3s^3)^{1/3}}\,\mathrm{d}s + z_0^2\frac{r^{10/3}}{r_0^{10/3}}\left(\frac{3-5r_0^2+2r_0^5}{3-5r^2+2r^5}\right)^{2/3}, \tag{3.18}$$

where $r_0 = \sqrt{x_0^2+y_0^2+z_0^2}$. Particle trajectories are determined by simultaneously solving (intersecting these surfaces) these equations to obtain a curve relating (x, y, z).

Figure 3 shows the separation surfaces in the flow. As shown in this figure, there is a region off the x–z plane between the separation surfaces, where the flow is blocked. The vertical plane in this figure shows the cross-section of the blocking region. The area of this cross-section in the limit of $x \to \pm\infty$ will be discussed in §3.5. Figures 4(a) and 4(b) show the stagnation lines close to the sphere and how they connect to the fixed points in the fluid. In this case, the fixed points are the y-axis outside of the sphere. This curve of fixed points is a subset of the original $z=0$ plane of fixed points present in the absence of the rigid sphere. From figure 4(b), it is easy to see that they are hyperbolic fixed points.

3.3. *Stagnation points on the sphere*

Since all points on a solid boundary are fixed points of the flow, special care is needed to define stagnation points which reside on a solid boundary. This degeneracy on

https://doi.org/10.1017/S0022112010004933 Published online by Cambridge University Press

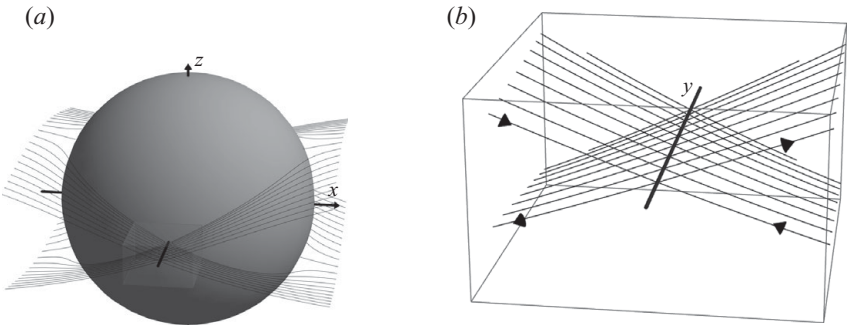


FIGURE 4. (a) Streamlines on separation surface close to the sphere. (b) A zoomed-in view of the cube near the y-axis.

solid boundaries may be split by computing those points on the boundary for which the linearization of the velocity vector field vanishes. These will define the stagnation points on the rigid boundary. Streamlines in the fluid which end at any stagnation point (whether in the fluid or on the boundary) are referred to as stagnation lines. Stagnation lines ending on the boundary are not necessarily perpendicular to the no-slip, rigid boundary. For a 2D flow, the angle between the stagnation line and the rigid surface can be computed, as seen in Pozrikidis (1997).

To find the stagnation points on the sphere, we linearize and rescale the velocity equation near the surface of the sphere. When the velocity field in spherical coordinates is linearized with respect to the radius r at 1, the expansions are

$$\frac{\mathrm{d}r}{\mathrm{d}t} = O((r-1)^2), \tag{3.19}$$

$$\frac{\mathrm{d}\theta}{\mathrm{d}t} = -4\cot\phi\sin\theta(r-1) + O((r-1)^2), \tag{3.20}$$

$$\frac{\mathrm{d}\phi}{\mathrm{d}t} = \frac{3+5\cos(2\phi)}{2}\cos\theta(r-1) + O((r-1)^2). \tag{3.21}$$

After rescaling the time $\tau = t(r-1)$ and neglecting the higher order, we reduce the ODE system to

$$\left.\begin{aligned} \frac{\mathrm{d}r}{\mathrm{d}\tau} &= 0, \\ \frac{\mathrm{d}\theta}{\mathrm{d}\tau} &= -4\cot\phi\sin\theta, \\ \frac{\mathrm{d}\phi}{\mathrm{d}\tau} &= \frac{3+5\cos(2\phi)}{2}\cos\theta. \end{aligned}\right\} \tag{3.22}$$

The steady state of the above ODE system provides the stagnation points, yielding the following conditions:

$$\cot\phi\sin\theta = 0, \qquad 2\cos\theta(5\cos^2\phi - 1) = 0. \tag{3.23}$$

Since $1 \leqslant r \leqslant \infty$, $0 \leqslant \phi \leqslant \pi$, $0 \leqslant \theta < 2\pi$, six stagnation points on the sphere are

$$r = 1, \begin{cases} \theta = 0, \pi, \\ \phi = \arccos\left(\dfrac{1}{\sqrt{5}}\right), \arccos\left(-\dfrac{1}{\sqrt{5}}\right), \end{cases} \quad \text{and} \quad \begin{cases} \theta = \dfrac{\pi}{2}, \dfrac{3\pi}{2}, \\ \phi = \dfrac{\pi}{2}. \end{cases} \tag{3.24}$$

https://doi.org/10.1017/S0022112010004933 Published online by Cambridge University Press

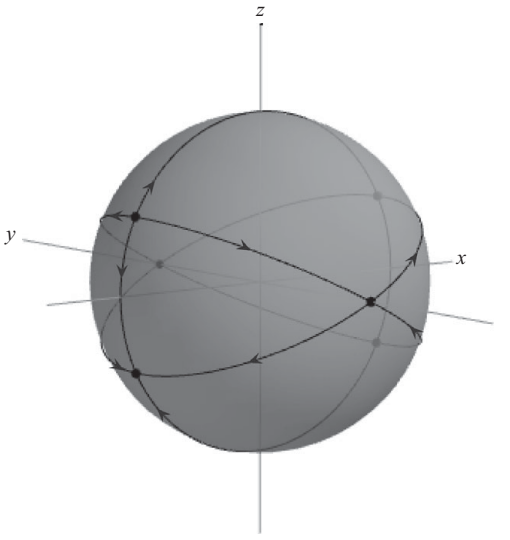


FIGURE 5. 'Footprint' of stagnation surfaces on the sphere.

Rewritten in rectangular coordinates, these points are located at

$$(0, \pm 1, 0) \quad \text{and} \quad \left(\pm\frac{2}{\sqrt{5}}, 0, \pm\frac{1}{\sqrt{5}}\right) \tag{3.25}$$

(the last points in the $y = 0$ symmetry plane are plotted in figure 2).

The rescaled velocity field provides an imprint of the particle trajectory pattern just off the sphere surface which mathematically reduces to heteroclinic connections between the stagnation points. These connections can be found from the ODE system (3.22),

$$\frac{\mathrm{d}\theta}{\mathrm{d}\phi} = -\frac{8\cot\phi\tan\theta}{3 + 5\cos(2\phi)}, \tag{3.26}$$

and the solution is

$$\sin^2\theta = C\frac{4\cos^2\phi - \sin^2\phi}{\sin^2\phi} = C\frac{5\cos^2\phi - 1}{\sin^2\phi}, \tag{3.27}$$

where C is a constant depending on the initial value of r, θ and ϕ. When $r = 1$, using the stagnation points as initial conditions, we get the equation of the trajectories on the sphere in rectangular coordinates:

$$(x, y, z) = (\pm 2\cos\phi, \pm\sqrt{1 - 5\cos^2\phi}, \pm\cos\phi), \quad (\arccos(1/\sqrt{5}) < \phi < \pi/2). \tag{3.28}$$

Or, $r = 1$ and $\cos\theta = \pm 2\cot\phi$ in the spherical coordinates. These trajectories connect the stagnation points in the rescaled flow field and demonstrate the topological structure on the sphere (see figure 5). From these trajectories, in the rescaled coordinates, we classify these stagnation points on the sphere as four nodal points (in the symmetry plane) and two hyperbolic points (on the y-axis). We emphasize that the rescaled flows are a projection onto the sphere, and all of these fixed points in the rescaled system correspond to higher-order (quadratic) hyperbolic points in the original system. We further remark that the entire y-axis exterior to the sphere is a line of fixed points. For finite values along the y-axis, this line is hyperbolic (in the

https://doi.org/10.1017/S0022112010004933 Published online by Cambridge University Press

x–z plane) with orientation depending upon the distance from the sphere. Infinitely far from the sphere along the y-axis, these fixed points lose their hyperbolic structure, with the flow becoming a simple shear flow (the background flow). In this limit, the orientation angle tends to zero. In the opposite limit approaching the sphere, this line of hyperbolic points tends to the higher-order hyperbolic fixed point on the sphere, with orientation angle depicted by the geodesic curves in figure 5, with a tangent value 4/3.

3.4. *Stagnation lines*

The precise mathematical definition of the blocked region requires some care to set up. Clearly, the unblocking and blocking regions are divided by the separation surfaces created by stagnation lines in the interior of the fluid as depicted in figures 2 and 3. These regions may be succinctly defined as follows. We define the set of unblocked trajectories to be the set of initial points whose particle trajectories intersect the $x=0$ plane off of the y-axis in finite or infinite time. This set of points is topologically open. The complement of this set (thus closed), we define to be the blocking region. Notice that the boundary of this set defines the separation surface. This connected surface contains the separating surface in the fluid, the y-axis, and the sphere surface.

To calculate this separation surface, we first identify the stagnation lines using the explicit formulae for the trajectory equations given in (3.9) and (3.12), then study their properties on and off the $y=0$ symmetry plane. Through this analysis, we will prove that the height $|z|$ of stagnation lines is finite as $x\to\pm\infty$ and y fixed.

3.4.1. *Stagnation lines in the $y=0$ symmetry plane*

Since one velocity component vanishes in this plane, streamlines are only governed by (3.12)

$$z^2=\frac{1}{\left(\dfrac{3}{2r^5}-\dfrac{5}{2r^3}+1\right)^{2/3}}\left(\int^{1/r}\frac{(1+s)(1-s)^{1/3}}{\left(1+2s+3s^2+\dfrac{3}{2}s^3\right)^{1/3}}\,\mathrm{d}s+C\right),\tag{3.29}$$

where C is determined by the initial value $(x_0, 0, z_0)$.

As we know from the previous subsection, four stagnation points on the sphere in this symmetry plane are $(\pm 2/\sqrt{5}, 0, \pm 1/\sqrt{5})$. We use these points as the initial value and get the equation of the stagnation line in this plane

$$z^2=\frac{1}{\left(\dfrac{3}{2r^5}-\dfrac{5}{2r^3}+1\right)^{2/3}}\int_{1/r}^{1}\frac{(1+s)(1-s)^{1/3}}{\left(1+2s+3s^2+\dfrac{3}{2}s^3\right)^{1/3}}\,\mathrm{d}s.\tag{3.30}$$

A few remarks regarding this stagnation line may be made. First, the height, z, of the stagnation line is bounded. This is easily seen by replacing the denominator in the integrand by unity and evaluating the integral. This gives a constant slightly bigger than the unit sphere radius. Second, this bound may be improved substantially through dividing the integral into subintervals and further integrand estimates (Zhao 2010). In fact, this ultimately establishes very tight upper and lower bounds for the limiting height value of the stagnation line in the limit $x\to\infty$. This upper bound is less than unity, with value 0.8831, and the lower bound is 0.8811. Numerically, we find

$$|z_{max}|\approx 0.88207\quad\text{as}\quad r\to\infty.\tag{3.31}$$

https://doi.org/10.1017/S0022112010004933 Published online by Cambridge University Press

3.4.2. *Stagnation lines off the $y=0$ symmetry plane*

We next calculate the stagnation surface out of the symmetry plane. As shown above, the set of fixed points which are detached from the sphere is the y-axis. Thus, any stagnation line not in the symmetry plane must contain a unique point on the y-axis (as shown in figures 3 and 4, which demonstrate this fact). We use these fixed points as the initial condition $r_0 = y_0 > 1$, $z_0 = 0$, and substitute them into the parametric equations for the fluid particle trajectory to obtain stagnation lines lying outside of the symmetry plane

$$y = y_0 \frac{r^{5/3}\,(y_0-1)^{2/3}\left(3+6y_0+4y_0^2+2y_0^3\right)^{1/3}}{y_0^{5/3}(r-1)^{2/3}(3+6r+4r^2+2r^3)^{1/3}}, \tag{3.32}$$

$$z^2 = \frac{2r^{10/3}}{\left(3-5r^2+2r^5\right)^{2/3}} \int_{1/r}^{1/y_0} \frac{(1+s)(1-s)^{1/3}}{\left(2+4s+6s^2+3s^3\right)^{1/3}}\,\mathrm{d}s. \tag{3.33}$$

This provides the equations for the stagnation lines out of the symmetry plane.

Notice that the stagnation line in the symmetry plane terminates on the sphere at a point which is not on the y-axis. Thus, next we investigate how the points on the separation surface close to the symmetry plane topologically connect stagnation lines intersecting the y-axis with the stagnation line in the symmetry plane. (Because of the symmetry of the flow, we only consider the case of y_0 close to $+1$.)

Using the y-coordinate of the stagnation lines crossing the y-axis given in (3.32), with an initial condition $(0, 1+\delta, 0)$ ($\delta \ll 1$), which is a point close to $(0, 1, 0)$, we have

$$y = \left(\frac{\delta^2(15+20\delta+10\delta^2+2\delta^3)}{2(1+\delta)^2}\right)^{1/3} \left(1-\frac{1}{r}\right)^{-2/3} \left(1+\frac{2}{r}+\frac{3}{r^2}+\frac{3}{2r^3}\right)^{-1/3}. \tag{3.34}$$

As $r \to \infty$, this limits to

$$\left(\frac{15}{2}\right)^{1/3} \delta^{2/3} \frac{\left(1+\dfrac{4\delta}{3}+\dfrac{2}{3}\delta^2+\dfrac{2}{15}\delta^3\right)^{1/3}}{(1+\delta)^{2/3}}, \tag{3.35}$$

and, as $\delta \to 0$, the leading-order approximation is $(15/2)^{1/3}\,\delta^{2/3}$. This shows that the out of the symmetry plane stagnation line crossing the fixed point $(0, y_0, 0)$, which is sufficiently close to the stagnation point $(0, 1, 0)$ on the sphere, asymptotically approaches the stagnation line in the $y=0$ plane as $r \to \infty$ (we note that the z-value given in (3.33) trivially converges in this limit to the limiting height computed above). This property guarantees that the blocking region at $x=\infty$ is completely characterized by the separation lines which intersect the y-axis. This will be very useful in measuring the cross-sectional area of the blocking region.

3.5. *Cross-sectional area of the blocking region as $x \to \infty$*

We next study the geometry of this blocking region far from the body. We do this by examining its cross-sectional structure (as in figures 3 and 6).

Unfortunately, at finite distances from the body, this cross-sectional region of intersecting the plane $x=L$ with the stagnation surface is not readily provided by the equations in (3.32) and (3.33) as they are parametrized by the spherical radius. Fortunately, we can overcome this difficulty by working with $L \to \infty$ since $r \sim x$ in this limit. In this limit, the formulae in (3.32) and (3.33) provide (y, z) coordinates for the curves bounding the blocking region (shown for large, but finite L, in figure 6). While from this figure it is clear that the height $z=z(y)$ will decay to zero as $y \to \infty$, the limiting procedure yields a parametric representation (with parameter y_0) for this

https://doi.org/10.1017/S0022112010004933 Published online by Cambridge University Press

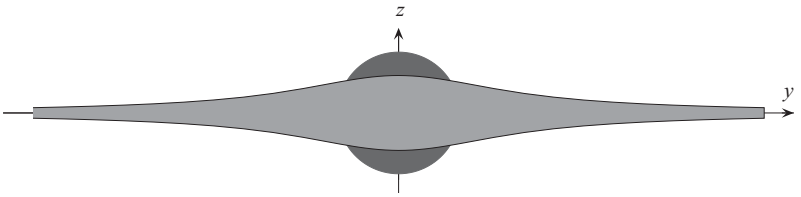


FIGURE 6. Cross-section of the bounded blocking region at infinity (viewed from upstream).

curve. To obtain the decay rate of $z(y)$ as $y \to \infty$ (which is critical to determine if the cross-sectional area is infinite) requires further analysis, as we next show.

From the equations of the stagnation lines (3.32) and (3.33), we get

$$y \sim y_0 \left(1 - \frac{1}{y_0}\right)^{2/3} \left(1 + \frac{2}{y_0} + \frac{3}{y_0^2} + \frac{3}{2y_0^3}\right)^{1/3}, \tag{3.36}$$

$$z^2 \sim \int_0^{1/y_0} \frac{(1+s)(1-s)^{1/3}}{\left(1 + 2s + 3s^2 + \frac{3}{2}s^3\right)^{1/3}} \, \mathrm{d}s = (z_\infty)^2, \tag{3.37}$$

as $r \to \infty$ by taking $x \to \infty$, where $z_\infty > 0$. Here y_0, a point on the y-axis, parametrizes the trajectory determined by the equations for y and z above. This parametric representation for the curve $z = z(y)$ may be viewed as an image of the y-axis under the flow after infinite time, which we may use to derive an explicit expression for the cross-sectional area. To wit, the Jacobian matrix for this mapping is

$$\frac{\mathrm{d}y}{\mathrm{d}y_0} = \left(1 + \frac{3}{2y_0^5} - \frac{5}{2y_0^3}\right)^{1/3} + \frac{5\,(1+y_0)}{2y_0^4 \left(1 - \frac{1}{y_0}\right)^{1/3} \left(2 + \frac{4}{y_0} + \frac{6}{y_0^2} + \frac{3}{y_0^3}\right)^{2/3}}. \tag{3.38}$$

The area of the blocked flow is noted as I,

$$\begin{aligned} \frac{I}{4} &= \int_0^\infty z(y)\,\mathrm{d}y = \int_1^\infty z_\infty(y_0) \frac{\mathrm{d}y}{\mathrm{d}y_0}\,\mathrm{d}y_0 \\ &= \int_1^\infty z_\infty \left(1 + \frac{3}{2y_0^5} - \frac{5}{2y_0^3}\right)^{1/3} \mathrm{d}y_0 \\ &\quad + \int_1^\infty z_\infty \frac{5\,(1+y_0)}{2y_0^4 \left(1 - \frac{1}{y_0}\right)^{1/3} \left(2 + \frac{4}{y_0} + \frac{6}{y_0^2} + \frac{3}{y_0^3}\right)^{2/3}} \mathrm{d}y_0 \\ &= \text{part 1} + \text{part 2}. \end{aligned} \tag{3.39}$$

For the integral part 2, the leading order of the integrand

$$\frac{5\,(1+y_0)}{2y_0^4 \left(1 - \frac{1}{y_0}\right)^{1/3} \left(2 + \frac{4}{y_0} + \frac{6}{y_0^2} + \frac{3}{y_0^3}\right)^{2/3}} \tag{3.40}$$

is

$$\frac{5}{2\,(2)^{2/3}\, y_0^3} \tag{3.41}$$

as $y_0 \to \infty$. Notice that the integrand in (3.37) is bounded. Consequently, an upper bound for the decay of z_∞ is $\sqrt{1/y_0}$ as $y_0 \to \infty$. Thus, the integral part 2 is bounded.

https://doi.org/10.1017/S0022112010004933 Published online by Cambridge University Press

We next show that the integral part 1 diverges:

$$\text{Part } 1 = \int_1^\infty z_\infty \left(1 - \frac{5}{2y_0^3} + \frac{3}{2y_0^5}\right)^{1/3} \mathrm{d}y_0. \tag{3.42}$$

Substitute $z_\infty(y_0)$ in (3.37) into the integrand

$$\text{Part } 1 = \int_1^\infty \left(\int_0^{1/y_0} \frac{(1+s)(1-s)^{1/3}}{\left(1 + 2s + 3s^2 + \frac{3}{2}s^3\right)^{1/3}} \mathrm{d}s \right)^{1/2} \left(1 - \frac{5}{2y_0^3} + \frac{3}{2y_0^5}\right)^{1/3} \mathrm{d}y_0. \tag{3.43}$$

As $y_0 \to \infty$,

$$\left(1 - \frac{5}{2y_0^3} + \frac{3}{2y_0^5}\right)^{1/3} \to 1. \tag{3.44}$$

Using the following result to estimate the integral in the kernel (which follows directly through straightforward Taylor expansion),

$$\int_0^\eta \frac{(1+s)(1-s)^{1/3}}{\left(1 + 2s + 3s^2 + \frac{3}{2}s^3\right)^{1/3}} \mathrm{d}s = \eta - \frac{\eta^3}{3} + O(\eta^4). \tag{3.45}$$

This establishes the following asymptotic expansion:

$$\int_0^{1/y_0} \frac{(1+s)(1-s)^{1/3}}{\left(1 + 2s + 3s^2 + \frac{3}{2}s^3\right)^{1/3}} \mathrm{d}s \sim \frac{1}{y_0} \quad \text{as} \quad y_0 \to \infty. \tag{3.46}$$

Therefore, the integrand of part 1 is asymptotic to $\sqrt{1/y_0}$ as $y_0 \to \infty$. With such a decay rate, the integral $\int_1^\infty \sqrt{1/y_0}\, \mathrm{d}y_0 = \infty$ is divergent. Since the integrand is sign definite, this result shows that part 1 is divergent. Consequently, the total area of the cross-section of the blocking region is infinite when the plane $x = x_0 \to \infty$.

In the y–z plane (i.e. $x = 0$), the blocking region is the y-axis, i.e. the area of the cross-section is zero. This is in sharp contrast with the calculation just presented above, where it was shown that at $x = \infty$, the cross-section of the blocking region is infinite. Since the explicit, closed-form formula for the area at an arbitrary distance from the sphere is not available, we study its behaviour by analysing the integrand involved here under different asymptotic limits. We will see a continuous connection between zero cross-sectional blocking area at $x = 0$ and diverging cross-sectional blocking area as $x \to \infty$.

The separation surface is generated by the stagnation lines crossing the fixed points $(0, y_0, 0)$ on the y-axis, where $|y_0| > 1$. If we take the cross-section of the blocking region at x_0, then $y^2 + z^2 = r^2 - x_0^2$. On the basis of the trajectory equations (3.32) and (3.33), we have

$$\left(\frac{3}{2}\frac{1}{r^5} - \frac{5}{2}\frac{1}{r^3} + 1\right)^{2/3} \left(r^2 - x_0^2\right) = \int_{1/r}^{1/y_0} \frac{(s+1)(1-s)^{1/3}}{\left(\frac{3}{2}s^3 + 3s^2 + 2s + 1\right)^{1/3}} \mathrm{d}s + y_0^2 \left(\frac{3}{2}\frac{1}{y_0^5} - \frac{5}{2}\frac{1}{y_0^3} + 1\right)^{2/3}. \tag{3.47}$$

https://doi.org/10.1017/S0022112010004933 Published online by Cambridge University Press

From the above equation, we find the mapping from r to y_0 with x_0 fixed. With such a mapping, the boundary of the cross-section of the blocking area can be written as parametric functions

$$\left.\begin{aligned} y &= y\left(r\left(y_0\right), y_0\right) \\ z &= z\left(r\left(y_0\right), y_0\right) \end{aligned}\right\} \tag{3.48}$$

at $x = x_0$ fixed. The leading-order asymptotic solution to (3.47) is

$$r \sim \sqrt{y_0^2 + x_0^2} \quad \text{as } y_0 \to \infty \quad \text{and} \quad x_0 \text{ fixed.} \tag{3.49}$$

If $\boldsymbol{a} = (0, z)$ and $\boldsymbol{n}$ is the outer normal direction of the cross-section,

$$\boldsymbol{a} \cdot \boldsymbol{n} = \frac{z(y_0)\dfrac{\mathrm{d}y}{\mathrm{d}y_0}}{\left|\dfrac{\mathrm{d}y}{\mathrm{d}y_0}\right|}. \tag{3.50}$$

By the divergence theorem or Gauss' theorem, the cross-section of the blocking area I is an explicit integral:

$$\frac{I}{4} = \int_\Omega \mathrm{d}A = \int_\Omega \operatorname{div} \boldsymbol{a}\, \mathrm{d}A = \int_{\partial\Omega} \boldsymbol{a} \cdot \boldsymbol{n}\, \mathrm{d}s = \int_1^\infty \left(z(y_0)\frac{\mathrm{d}y}{\mathrm{d}y_0}\right) \mathrm{d}y_0. \tag{3.51}$$

From the asymptotic result (3.49) and several applications of the implicit function theorem to obtain derivative asymptotics (we relegate these technical details to Appendix A), we find that for finite x_0, the integrand decays as $x_0/(\sqrt{2}y_0^{3/2})$, when $y_0 \to \infty$, which yields a finite cross-sectional blocking area.

To study the behaviour for the blocking area as x_0 increases, we take the cross-section at $x_0 = y_0^\epsilon$, where $\epsilon > 0$ is a constant.

(i) When $0 < \epsilon < 1$, from (3.47), we find $r \sim \sqrt{y_0^2 + y_0^{2\epsilon}}$ as $y_0 \to \infty$. Substitute this into the integrand for the blocking area, the integrand for the blocking area is asymptotic to $(1/\sqrt{2})(1/y_0^{3/2-\epsilon})$. When $0 < \epsilon < 1/2$, the integral is convergent. Otherwise, $1/2 < \epsilon < 1$, the integral is divergent.

(ii) If the cross-section is taken at $x_0 = y_0^\epsilon$ ($\epsilon \geqslant 1$), then $r \sim \sqrt{y_0^{2\epsilon} + y_0^2}$ as $y_0 \to \infty$. In this case, the integrand of (3.51) for the blocking area decays as $3/(2\sqrt{y_0})$ as $y_0 \to \infty$.

This illustrates an unreported property about the solution of the Stokes flow but physically not observed. Since, at large distance, the characteristic length used in the Reynolds number need to be redefined, the inertia terms ignored in the Navier–Stokes equation are not negligible.

4. Shear past a sphere whose centre off the zero-velocity plane of the primary shear flow

When the centre of the unit sphere $x^2 + y^2 + z^2 = 1$ is out of the zero-velocity plane of the background shear flow illustrated in figure 1, the non-dimensional primary linear shear flow can be written as $\boldsymbol{U} = z\boldsymbol{e}_x + U\boldsymbol{e}_x$, in which the uniform flow rate U is related to the shear rate and the distance between the centre of the sphere and the zero-velocity plane of the shear flow. Without loss the generality, we can assume $U > 0$. While we will not be able to obtain a closed-form explicit solution in these off-centre cases as before, we will explicitly compute the fixed-point structure in closed form.

https://doi.org/10.1017/S0022112010004933 Published online by Cambridge University Press

The exact velocity field for the flow is given in (2.5). We rewrite the velocity field as an ODE system in spherical coordinates:

$$\left.\begin{aligned}
\frac{\mathrm{d}r}{\mathrm{d}t} &= \frac{Ur(1+2r)+(3+6r+4r^2+2r^3)\cos\phi}{2r^4}(r-1)^2\cos\theta\sin\phi,\\
\frac{\mathrm{d}\theta}{\mathrm{d}t} &= \frac{Ur(1+3r^2-4r^3)+2(1+r^2-2r^5)\cos\phi}{4r^5\sin\phi}\sin\theta,\\
\frac{\mathrm{d}\phi}{\mathrm{d}t} &= -\frac{Ur(1+3r^2-4r^3)\cos\phi+4(1-r^5)\cos^2\phi+2(r^2-1)}{4r^5}\cos\theta,
\end{aligned}\right\} \tag{4.1}$$

where $1\leqslant r<\infty$, $0\leqslant\phi\leqslant\pi$ and $0\leqslant\theta<2\pi$. From the above ODE system (4.1), we apply the same approach as we have used in the previous section to attain the ODEs $\mathrm{d}y/\mathrm{d}r$ and $\mathrm{d}z/\mathrm{d}r$. Skipping the details of changing variables and taking derivatives, we get $\mathrm{d}y/\mathrm{d}r$ and $\mathrm{d}z/\mathrm{d}r$ with the radius r as a new independent variable:

$$\frac{\mathrm{d}y}{\mathrm{d}r}=\frac{(1+r)\left(3r^2U+10z\right)y}{2(1-r)r\left[r^2(1+2r)U+\left(3+6r+4r^2+2r^3\right)z\right]}, \tag{4.2}$$

$$\frac{\mathrm{d}z}{\mathrm{d}r}=\frac{(1+r)\left(3Uz+10\dfrac{z^2}{r^2}-2\right)}{2(1-r)\left[r(1+2r)U+\left(3+6r+4r^2+2r^3\right)\dfrac{z}{r}\right]}, \tag{4.3}$$

and $x=\sqrt{r^2-y^2-z^2}$. Here, $\mathrm{d}y/\mathrm{d}r$ and $\mathrm{d}z/\mathrm{d}r$ are no longer decoupled as in the first case, though $\mathrm{d}z/\mathrm{d}r$ is independent of y. For this case, we have not found the fluid particle trajectories explicitly, but (4.2) and (4.3) are crucial for determining the bifurcation diagrams of the flow.

To demonstrate the flow structures, we plot trajectories of fluid particles with different uniform flow rates U. Figures 7(a) and 7(b) show the trajectories of fluid particles in three dimensions when the centre of the sphere is in the zero-velocity plane of the background shear flow ($U=0$), the case in the previous section; figures 7(c) and 7(d) show the trajectories with a different background flow ($U=1$), and figure 8 is for $U=3$ in the background shear flow.

4.1. *Bifurcation of streamlines and stagnation points on the sphere*

From (4.1), we find the analytical formulae of the stagnation points on the sphere and the fixed points in the interior of the fluid. As U varies, the curves of fixed points in the interior of the fluid deform and the location of the stagnation points on the sphere changes. The curves of the fixed points are always in the y–z plane. Figure 9 demonstrates bifurcation diagrams in the trajectories for four canonical stages and the transitions between them in the $y=0$ symmetry plane close to the sphere, as U increases. Critical uniform flow rates $U^{\star}$ and $U^{\star\star}$ are provided in the next subsection, after the general formula of fixed points are derived.

For stage 1, figure 9(a) shows the diagram of streamlines in the symmetry plane below the sphere when $U<U^{\star}$. The stagnation line bounding the blocking region moves downward with the stagnation points on the sphere, as the centre of the sphere moves upwards from the zero-velocity plane of the background shear. There is no fixed point in the interior of the fluid in this symmetry plane for this stage. The fixed points in the interior of the fluid are on two curves in the y–z plane.

The transition from stage 1 to stage 2 appears when $U=U^{\star}$, when a cubic parabolic fixed point (a cusp point) emerges in the symmetry plane (figure 9b). In stage 2

https://doi.org/10.1017/S0022112010004933 Published online by Cambridge University Press

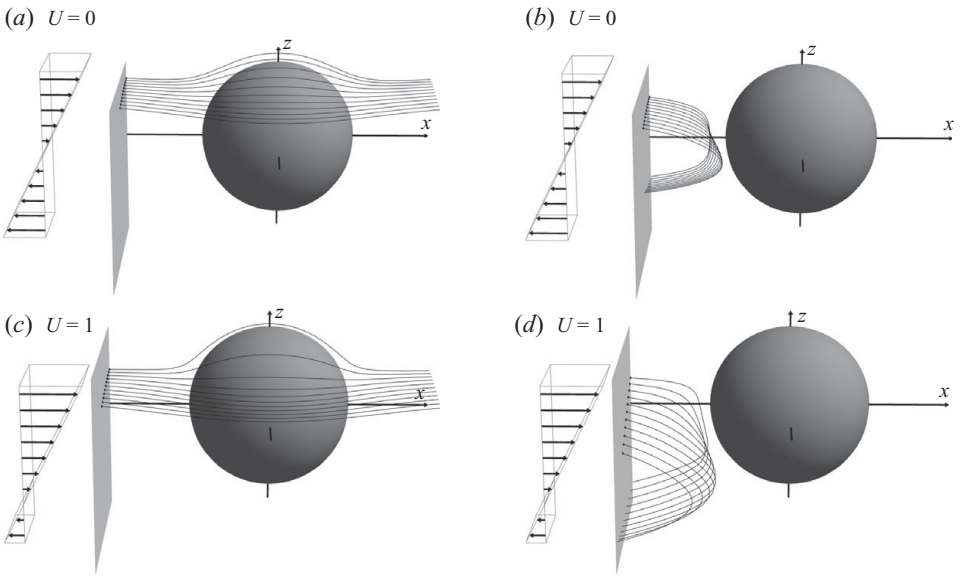


FIGURE 7. Three-dimensional fluid particle trajectories either passing the sphere or being blocked by it, depending on different values of U for the background shear flow.

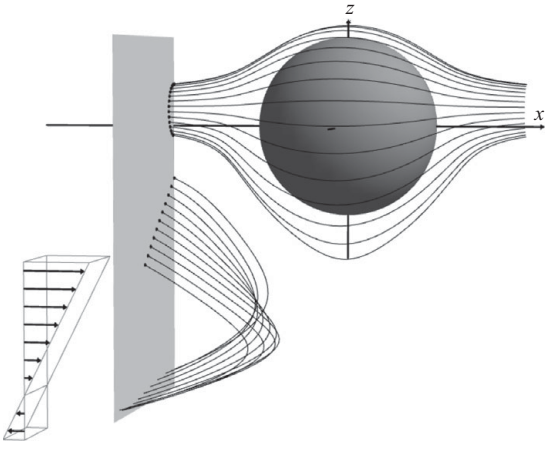


FIGURE 8. Trajectories of the fluid particles starting from the initial conditions (marked by dots) for the value $U = 3$.

($U^\star < U < U^{\star\star}$), this cubic parabolic fixed point deforms into a pair of fixed points, one elliptical fixed point and one hyperbolic fixed point, in the symmetry plane. Surrounding the elliptical fixed point, there are closed orbits in the symmetry plane plotted in figure 9(c).

The transition from stage 2 to stage 3 occurs when $U = U^{\star\star}$. With this critical value, the stagnation lines separating the blocking region also form a separatrix distinguishing the open trajectories from the closed trajectories below the sphere. These stagnation lines cross the hyperbolic fixed point and end on the stagnation point on the sphere. Above the hyperbolic fixed point, streamlines are closed; below it, the streamlines are open and fluid particles pass the sphere from the right to the

https://doi.org/10.1017/S0022112010004933 Published online by Cambridge University Press

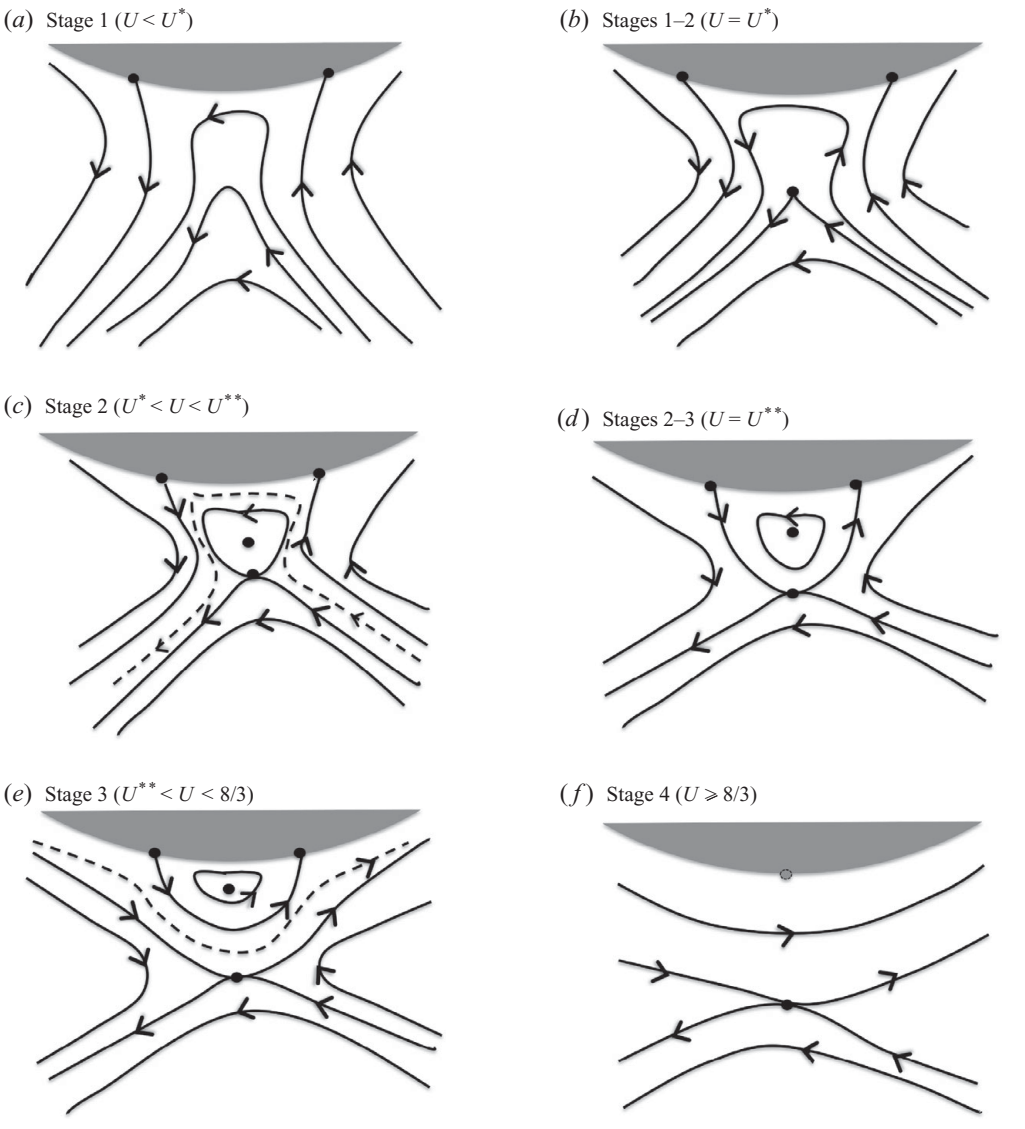


FIGURE 9. (*a–f*) Sketches of the bifurcation sequence below the sphere in the $y = 0$ symmetry plane as U, the uniform flow rate, increases. The grey regions are part of the sphere. Solid dots indicate stagnation points on the sphere or fixed points in the interior of the fluid. Arrows show the direction of the flow along the trajectories.

left. There is no flow past the sphere from the left to the right below the sphere in this symmetry plane.

In stage 3 ($U^{**} < U < 8/3$) in figure 9(*e*), the elliptical fixed point moves towards the sphere. The stagnation lines ending on the hyperbolic fixed points are no longer separation lines of the elliptical fixed points. The closed orbits around the elliptical fixed point are above the blocking region in this symmetry plane. There are open streamlines between the elliptical fixed point and the hyperbolic point. Fluid particles along the open streamlines pass the sphere from the left to the right above the hyperbolic fixed points.

https://doi.org/10.1017/S0022112010004933 Published online by Cambridge University Press

Stage 4 begins at $U = 8/3$, when the elliptic fixed point, the two stagnation points in the symmetry plane on the sphere, and two stagnation points out of the symmetry plane vanish or collapse simultaneously at the open dot shown in figure 9(*f*). After these four stagnation points on the sphere and the elliptical fixed point in the interior of the fluid collapse, the flow structure remains the same as shown in figure 9(*f*), with only two stagnation points on the sphere.

A brief discussion on dynamical system theory is merited. For example, there is a criterion (Poincaré–Bendixson) which states that a two-dimensional non-divergence-free vector field may possess periodic particle trajectories only if the divergence of the flow changes sign. In the symmetry plane, we have a two-dimensional compressible flow for all values of the parameter U. For some values of this parameter, we just document the existence of closed orbits in the symmetry plane. A quick inspection of the divergence of the velocity field $(u(x, 0, z), w(x, 0, z))$ shows that indeed it does change sign, in agreement with the Poincaré–Bendixson criterion. Moreover, using the generalized Poincaré–Hopf index definition of Ma & Wang (2001), the index of the flow is also shown to be preserved, with the caveat that fixed points on the boundary are indexed with selected weight one-half.

4.2. *Stagnation points and fixed points in the interior of the fluid*

Next, we provide the explicit formula for the stagnation points on the sphere when its centre is out of the zero-velocity plane of the primary background shear flow. After linearizing, rescaling $\tau = t(r - 1)$ and neglecting the higher-order terms in the ODE system (4.1), we get

$$\frac{\mathrm{d}r}{\mathrm{d}\tau} = 0, \tag{4.4}$$

$$\frac{\mathrm{d}\theta}{\mathrm{d}\tau} = -\frac{3U + 8\cos\phi}{2\sin\phi}\sin\theta, \tag{4.5}$$

$$\frac{\mathrm{d}\phi}{\mathrm{d}\tau} = \frac{3 + 3U\cos\phi + 5\cos(2\phi)}{2}\cos\theta. \tag{4.6}$$

Based on the condition for stagnation points on the sphere,

$$\frac{\mathrm{d}\theta}{\mathrm{d}\tau} = 0 \quad \text{and} \quad \frac{\mathrm{d}\phi}{\mathrm{d}\tau} = 0, \tag{4.7}$$

the explicit formulae for stagnation points on the sphere are obtained as follows.

(i) When $0 \leqslant U < 8/3$, there are six solutions of (4.7)

$$\left.\begin{aligned} \theta &= 0, \pi \\ \phi &= \arccos\left(\frac{-3U \pm \sqrt{9U^2 + 80}}{20}\right) \end{aligned}\right\} \tag{4.8}$$

and

$$\left.\begin{aligned} \theta &= \frac{\pi}{2}, \frac{3\pi}{2} \\ \phi &= \arccos\left(-\frac{3U}{8}\right). \end{aligned}\right\} \tag{4.9}$$

https://doi.org/10.1017/S0022112010004933 Published online by Cambridge University Press

In rectangular coordinates, these six points are

$$\left(\pm\left(1-\left(\frac{\sqrt{9U^2+80}-3U}{20}\right)^2\right)^{1/2}, 0, \frac{\pm\sqrt{9U^2+80}-3U}{20}\right), \tag{4.10}$$

and

$$\left(0, \pm\sqrt{1-\left(\frac{3U}{8}\right)^2}, -\frac{3U}{8}\right). \tag{4.11}$$

As $U \to 8/3$, four of the stagnation points at the lower part of the sphere approach each other; at $U = 8/3$, they collapse and disappear, and there are two stagnation points

$$\left(\pm\frac{2\sqrt{6}}{5}, 0, \frac{1}{5}\right) \tag{4.12}$$

left on the sphere.

(ii) When $U \geqslant 8/3$, there are only two solutions of (4.7)

$$\left.\begin{aligned}\theta &= 0, \quad \pi,\\ \phi &= \arccos\left(\frac{\sqrt{9U^2+80}-3U}{20}\right)\end{aligned}\right\} \tag{4.13}$$

representing two stagnation points

$$\left(\pm\left(\frac{4}{5}+\frac{3U\left(\sqrt{9U^2+80}-3U\right)}{200}\right)^{1/2}, 0, \frac{\sqrt{9U^2+80}-3U}{20}\right) \tag{4.14}$$

on the sphere in rectangular coordinates.

Besides the stagnation points on the sphere, we find the explicit formula for all the fixed points in the interior of the fluid. As shown in the previous section, where the centre of the sphere is in the zero-velocity plane of the primary shear flow, i.e. $U = 0$ in the primary flow, the fixed points are on the y-axis. When $U \neq 0$, the curves for fixed points still only appear in the y–z plane but are no longer restricted to the y-axis. The fixed points in the interior of the fluid are found as functions of r and U from (4.2) and (4.3):

$$\left.\begin{aligned}x(r, U) &= 0,\\ z(r, U) &= -\frac{Ur^2(1+3r^2-4r^3)}{2(1+r^2-2r^5)},\\ y(r, U) &= \pm\sqrt{r^2-z^2(r, U)} = \pm\sqrt{r^2-\left(\frac{Ur^2}{2}\frac{(1+3r^2-4r^3)}{(1+r^2-2r^5)}\right)^2}.\end{aligned}\right\} \tag{4.15}$$

If $0 < U < U^\star$, the fixed points are on two curves. Each of them ends on one of the stagnation points

$$\left(\pm\left(1-\frac{\left(3U+\sqrt{9U^2+80}\right)^2}{400}\right)^{1/2}, 0, -\frac{\sqrt{9U^2+80}+3U}{20}\right) \tag{4.16}$$

https://doi.org/10.1017/S0022112010004933 Published online by Cambridge University Press

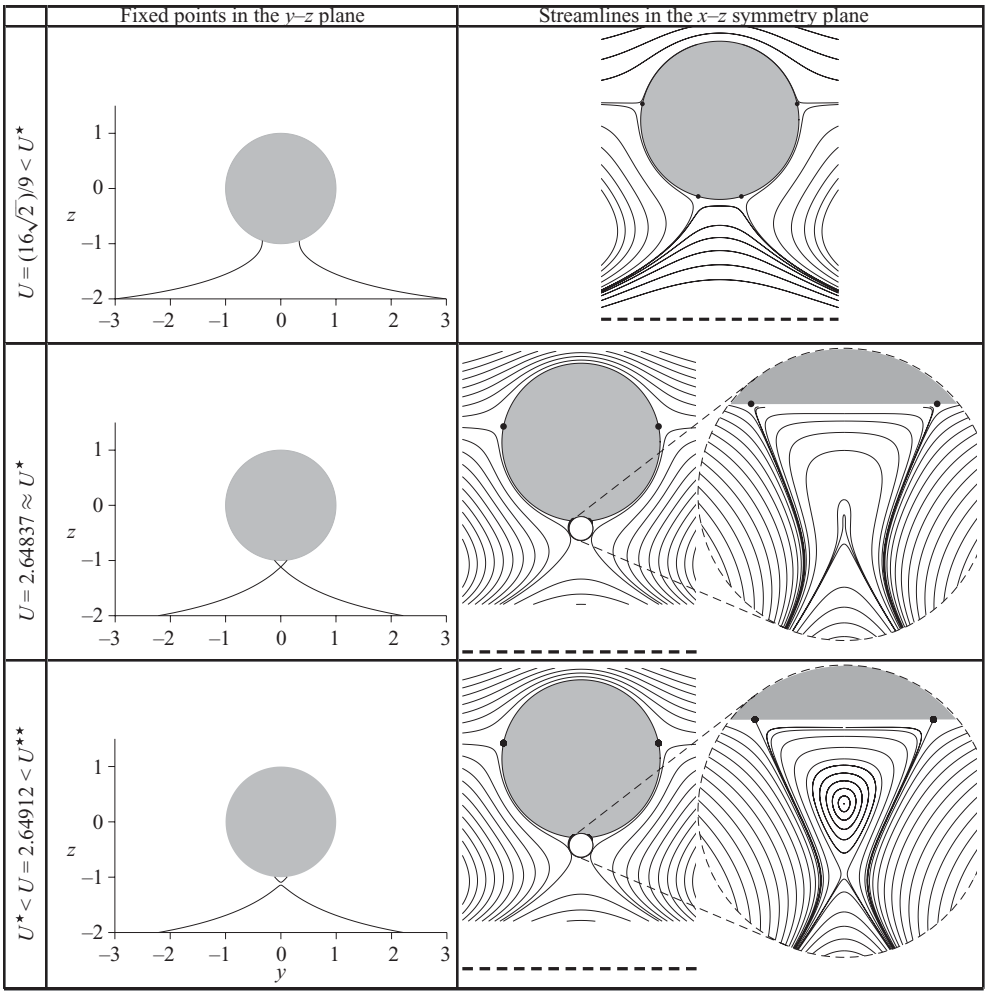


FIGURE 10. Fixed points in the interior of the fluid in the $x=0$ plane and streamlines in the $y=0$ symmetry plane for different values of U. The thick dashed lines in the streamline patterns indicate the zero-velocity plane of the primary background shear flow. The sphere is depicted in grey, with dots marking the stagnation points on the surface.

on the sphere. Far away from the sphere, these two curves are asymptotic to the line $(0, y, -U)$, which is in the zero-velocity plane of the background linear shear. On the other hand, closer to the sphere, as U increases, these two distinct curves of fixed points deform and intersect at a critical value of $U=U^\star$, as shown in the second column and row in figure 10. Before this critical value, a few other transitions in the graph of these curves are noteworthy. When $U \leqslant (16/9)\sqrt{2}$, the curves of fixed points in the y–z plane can be written as functions of y. When $U=(16/9)\sqrt{2}<U^\star$, the curve $(y(r, U), z(r, U))$ has a vertical tangent line at the stagnation point on the sphere.

The critical ratio $U^\star$ is equal to

$$\frac{2(1+s^2-2s^5)}{s(1+3s^2-4s^3)}, \tag{4.17}$$

https://doi.org/10.1017/S0022112010004933 Published online by Cambridge University Press

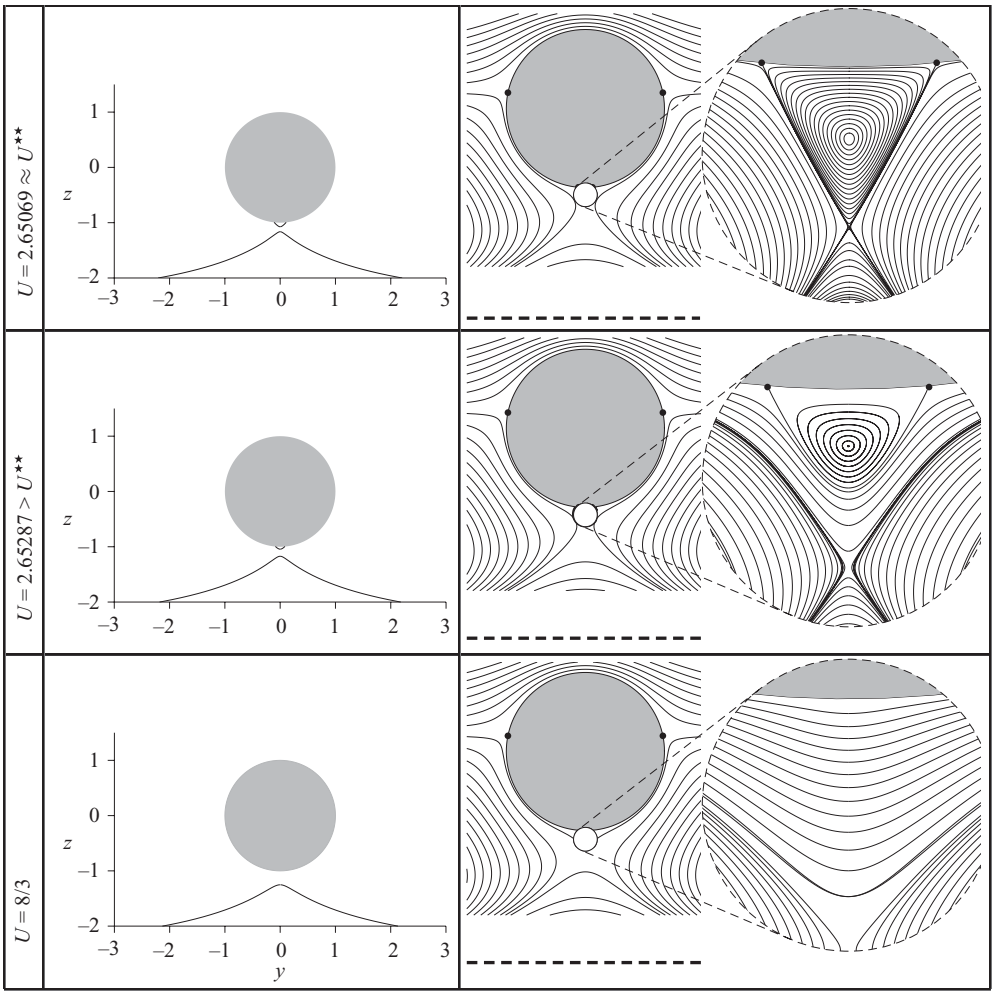


FIGURE 11. Continuation of figure 10.

where s is the smallest positive real root of the following polynomial:

$$8s^6 + 4s^5 - 4s^3 - 11s^2 - 2s - 1 = 0, \tag{4.18}$$

as derived from (4.15). At this critical ratio $U^\star$, two pieces of curves join at a cusp fixed point in the symmetry plane.

As U ($U^\star \leqslant U < 8/3$) increases further, these two curves of fixed points bifurcate into two new curves. One of the new curves has no end point on the sphere, and all points on this curve are hyperbolic fixed points. The other curve is a finite-length curve whose end points are two stagnation points on the sphere. Along this finite-length curve, the fixed points change properties as follows. First, near the two stagnation points on the sphere, i.e. near the two end points of the curve of fixed points, the curve consists of hyperbolic fixed points. Second, a little further down the curve, at a critical position these points become two degenerate fixed points with three vanishing eigenvalues. Finally, moving still further away from the sphere and close to

https://doi.org/10.1017/S0022112010004933 Published online by Cambridge University Press

the symmetry x–z plane, the points on this curve become elliptical fixed points and no further transition is observed through the symmetry plane. These properties are determined by the sign of the following function:

$$F(r, U) = 2[1 + r + 2r^2(1 + r + r^2)]^3 + U^2 r^4(5 + 3r + 24r^2 - 48r^3 - 84r^4 - 60r^5 - 44r^6 + 36r^7 + 24r^8) \quad (4.19)$$

and (4.15). This function, $F(r, U)$, is derived through a standard eigenanalysis. For given U and r, if $F(r, U) > 0$, the corresponding point (x, y, z) from (4.15) is a hyperbolic fixed point. If $F(r, U) < 0$, and the point (x, y, z) satisfying (4.15) is an elliptical fixed point. Otherwise, when $F(r, U) = 0$, the point of (4.15) is a higher-order fixed point with all three eigenvalues being zero.

When $U = 8/3$, the finite curve shrinks into a point and collapses with the four stagnation points on the sphere, and all the fixed points in the interior of the fluid are now on the infinite-length curve. After $U \geqslant 8/3$, fixed points in the interior of the fluid are always on such a curve.

The quantified streamline plots shown in figures 10 and 11 document the qualitative bifurcation sketches in figure 9. In figure 10, we show fixed point curves in the flow and the flow structure in the x–z symmetry plane with given U. Notice that the fixed points are plotted in the y–z plane, since the fixed points in the fluid are only in the y–z plane. In figures 10 and 11, the first column shows the different values of U studied, and the second column shows plots for curves of fixed points from (4.15) (the grey area indicates the sphere). The third column shows streamline patterns obtained numerically in the x–z symmetry plane, i.e. the lateral view.

The first value $U = (16/9)\sqrt{2} < U^\star$ is picked corresponding to stage 1 in the bifurcation sketches of figure 9. In this case, as shown in the second column, fixed points are on two infinite-length curves, each of whose end point is a stagnation point on the sphere. With this special value, the curves of fixed points in the y–z plane have infinite slope at the stagnation point. With the second value $U = 2.64837 \approx U^\star$, a cubic parabolic (cusp) fixed point appears. In the third row $U^\star < U = 2.64912 < U^{\star\star}$, the fixed points in the fluid are on two new curves. Both end points of the finite length curve are stagnation points on the sphere, and the curve with infinite length is asymptotic to a line in the zero-velocity plane of the background shear flow. With the fourth value $U = 2.65059 \approx U^{\star\star}$ in figure 11, the fixed points in the interior of the fluid are still on two curves. The stagnation lines in the streamline plot in the symmetry plane connect the hyperbolic fixed point in the fluid with the stagnation points on the sphere, and separate closed orbits around the elliptical fixed point from the open trajectories. For $U^{\star\star}$, we do not have an explicit formula for this value and use the numerical approximation 2.65059. For the fifth value $U^{\star\star} < U = 2.65287 < 8/3$, the elliptical fixed points moves up as U increases, and there are fluid particles which pass the sphere from the left to the right between the elliptical fixed point and the hyperbolic fixed point. The last case $U = 8/3$ shows that fixed points are on one curve in the interior of the fluid.

These numerical results clearly show the existence of the blocking regions when the sphere is out of the zero-velocity plane of the primary shear flow. The streamline plots in the $y = 0$ plane show the interesting bifurcation appearing in the fluid particle trajectories.

When $U^\star < U < 8/3$, streamlines show a 3D eddy near the elliptical fixed points below the sphere. Figure 12 shows the circulation near the elliptical fixed points below

https://doi.org/10.1017/S0022112010004933 Published online by Cambridge University Press

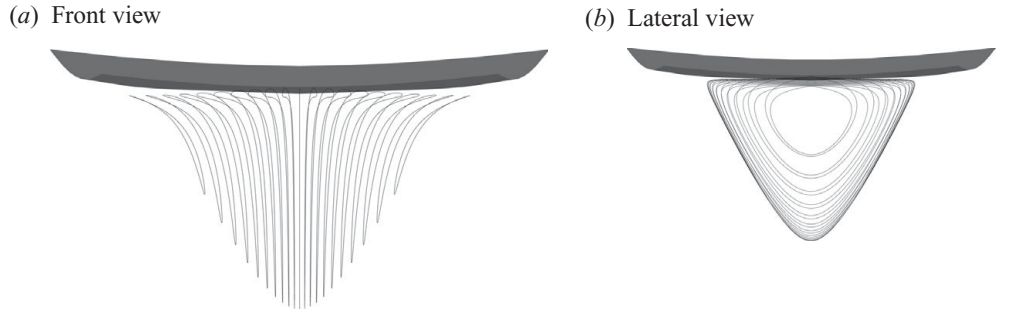


FIGURE 12. (*a, b*) Circulation near elliptical and hyperbolic fixed points below the sphere. Grey surface marks the surface of the sphere.

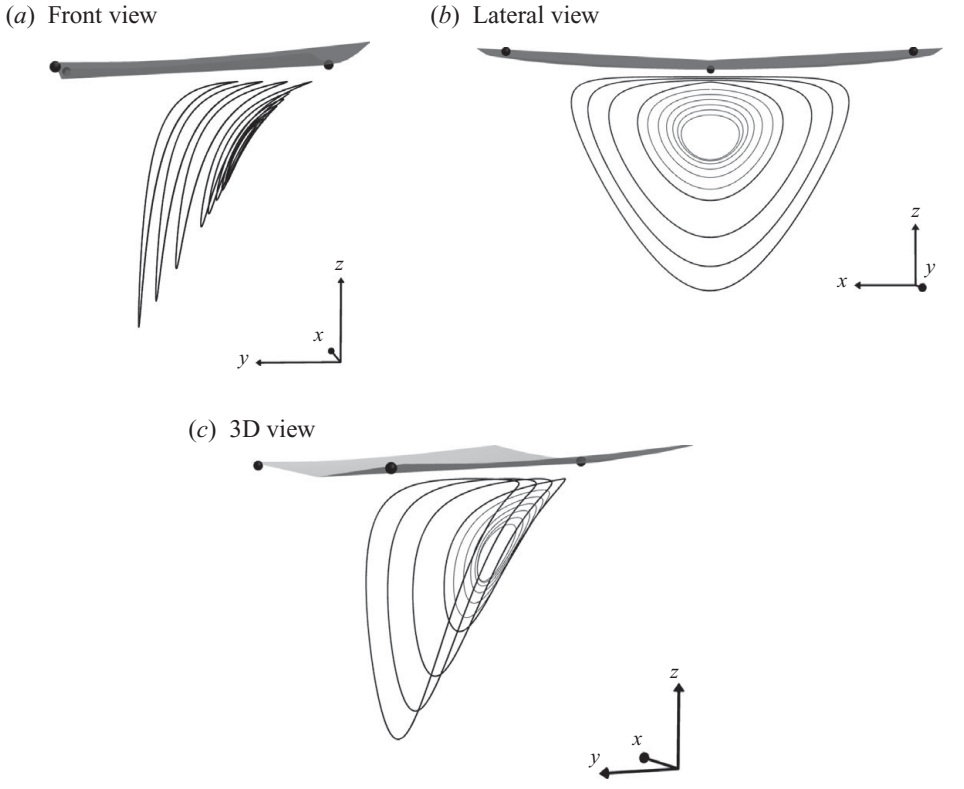


FIGURE 13. (*a–c*) Circulation near elliptical and hyperbolic fixed points below the sphere.

the sphere when $U = 2.6514$. Figure 12(*a*) is the front view of fluid particle trajectories and figure 12(*b*) is their lateral view. From figure 12(*b*), it is clear that these are closed trajectories circulating around the elliptical fixed points on the finite-length fixed point curve in and out of the symmetry plane. From the front view in Figures 12(*a*) and 13(*a*), we see that trajectories are further deformed when they are close to the surface of the sphere and approaching the hyperbolic fixed point on the finite-length fixed point curve.

https://doi.org/10.1017/S0022112010004933 Published online by Cambridge University Press

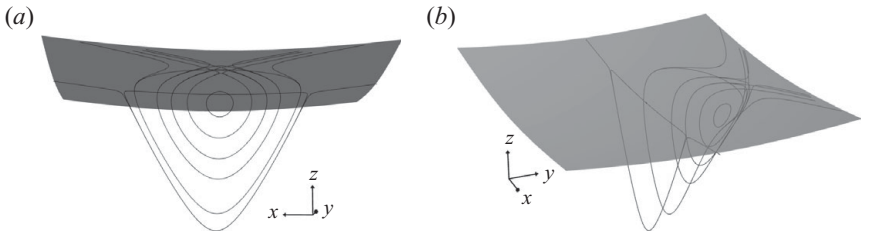


FIGURE 14. (*a, b*) Closed and open streamlines below the sphere exhibiting the streamline pattern bifurcation.

Figures 13 and 14 show streamlines in the $y < 0$ half-space below the sphere. In figure 13, the streamlines are only closed orbits near the fixed points on the finite-length curve (here we take $U = 2.6514$). Figure 13(a) is the front view, figure 13(b) is the lateral view, and figure 13(c) is the 3D view. These orbits are selected so that they are around the elliptical points, but near the sphere they are close to the hyperbolic fixed points on the finite-length fixed point curve. Figure 14 shows both closed and open streamlines near the fixed points.

5. A sphere embedded in rotating flows

To further explore similar phenomena, we next consider the flow with a sphere embedded in rotating flows. The centre of the sphere is set at the origin of the coordinate system. The background flow is a rigid-body rotation in the x–y plane with the rotation axis parallel to the z-axis and translated a fixed distance L from the origin. In this case, the x–y plane is the symmetry plane of the flow. The planar linear shear case with the sphere centre at some distance off the zero-velocity plane may be viewed as an extreme case of this rotating background flow in that at large distances L, the curvature of rigid-body rotation streamlines over regions of sphere radius scales becomes negligible. However, there are important differences with respect to the planar case in the interpretation of blocking regions for the case of a rotating background flow past a sphere, as in this case the definition of blocking itself becomes fundamentally different. We will study the case when the sphere is fixed in the rotating flow first and then allow the sphere to additionally self-rotate. For a sphere self-rotating in the rotating background flow, we report results about the flow in cases when the sphere may freely self-rotate and the cases when the sphere self-rotates at a prescribed angular velocity. The rotation axis of the self-rotation of the sphere is the z-axis. For a sphere embedded in such rotating flows, we will next find the explicit fluid particle trajectories from the exact velocity field and document the analytical formula for stagnation points on the sphere and the fixed points in the interior of the fluid.

5.1. *A fixed sphere in the rotating flow*

When the unit sphere is embedded in purely rotating flows, the background flow can be decomposed into a uniform flow plus two linear shear flows in rectangular coordinates, whose origin is the centre of the sphere. Assuming that the non-dimensional angular velocity of the rotation is $(0, 0, 1)$ and the distance between the rotation axis and theorigin is $L \geqslant 0$, the background flow is $y\boldsymbol{e}_x - (x + L)\boldsymbol{e}_y$. When the sphere is fixed,

https://doi.org/10.1017/S0022112010004933 Published online by Cambridge University Press

with no-slip boundary condition on the surface of the sphere, the velocity of the flow can be obtained from (2.4),

$$\left.\begin{aligned} u(x,y,z) &= \left(y - \frac{y}{\left(x^2+y^2+z^2\right)^{3/2}} + \frac{3Lxy}{4\left(x^2+y^2+z^2\right)^{3/2}} - \frac{3Lxy}{4\left(x^2+y^2+z^2\right)^{5/2}}\right), \\ v(x,y,z) &= -L - x + \frac{x}{\left(x^2+y^2+z^2\right)^{3/2}} \\ &\quad + \frac{L}{4}\left(\frac{3}{\sqrt{x^2+y^2+z^2}} + \frac{1+3y^2}{\left(x^2+y^2+z^2\right)^{3/2}} - \frac{3y^2}{\left(x^2+y^2+z^2\right)^{5/2}}\right), \\ w(x,y,z) &= -\frac{3Lyz}{4\left(x^2+y^2+z^2\right)^{5/2}} + \frac{3Lyz}{4\left(x^2+y^2+z^2\right)^{3/2}}. \end{aligned}\right\} \tag{5.1}$$

Similar to the planar shear past a sphere, we calculate the fluid particle trajectories for this velocity field by obtaining explicit formulae in terms of r,

$$x = \frac{r^2(5+4r)}{8L(1-r)} + \frac{r^2\left(27\sqrt{2}\log(2\sqrt{r}+\sqrt{2(1+2r)}) - 8C_1\right)}{16L(1-r)\sqrt{r(1+2r)}}, \tag{5.2}$$

$$z^2 = \frac{C_2 r^3}{(r-1)^2(1+2r)}, \tag{5.3}$$

$$y^2 = r^2 - x^2 - z^2, \tag{5.4}$$

where C_1 and C_2 are constants determined by the initial position of the fluid particle.

To present the structure of the flow, we plot fluid particle trajectories with different values of L in the x–y symmetry plane. When $L=0$, trajectories are shown in figure 15(a). In this case, it is clear from the velocity field (5.1) that there is no motion in the z-direction and all velocity components vanish along the z-axis ($x=y=0$). When $0<L<2$, trajectories are illustrated in figure 15(b) with a specified value $L=1$. There are two stagnation points on the sphere and they are in the x–z plane, shown in figure 17(b), where we show the stagnation points on the sphere. When $L=2$, trajectories are shown in figure 15(c). There is one stagnation point on the sphere at $(-1,0,0)$. When $L>2$, trajectories are plotted in figure 15(d) with $L=3$. There are two stagnation points on the sphere. Figure 16 is the 3D view of figure 15(d).

As figures 15 and 16 implied, the stagnation points on the sphere depend on the distance L. For a unit sphere, there are two stagnation points $(-L/2, 0, \sqrt{4-L^2}/2)$ and $(-L/2, 0, \sqrt{4-L^2}/2)$ on the sphere if $0 \leqslant L < 2$. When $L=2$, there is only one stagnation point $(-1,0,0)$ on the sphere. When $L>2$, there are still two stagnation points on the sphere at $(-2/L, (\sqrt{L^2-4}/L), 0)$ and $(-2/L, -(\sqrt{L^2-4}/L), 0)$, but they are in the x–y symmetry plane instead of the x–z plane for $L<2$.

Furthermore, we get the formula for fixed points in the interior of the fluid, which are only in the x–z plane. The implicit formula for fixed points in the fluid is

$$\frac{L+4x}{4\left(x^2+z^2\right)^{3/2}} = L + x - \frac{3L}{4\sqrt{x^2+z^2}}. \tag{5.5}$$

https://doi.org/10.1017/S0022112010004933 Published online by Cambridge University Press

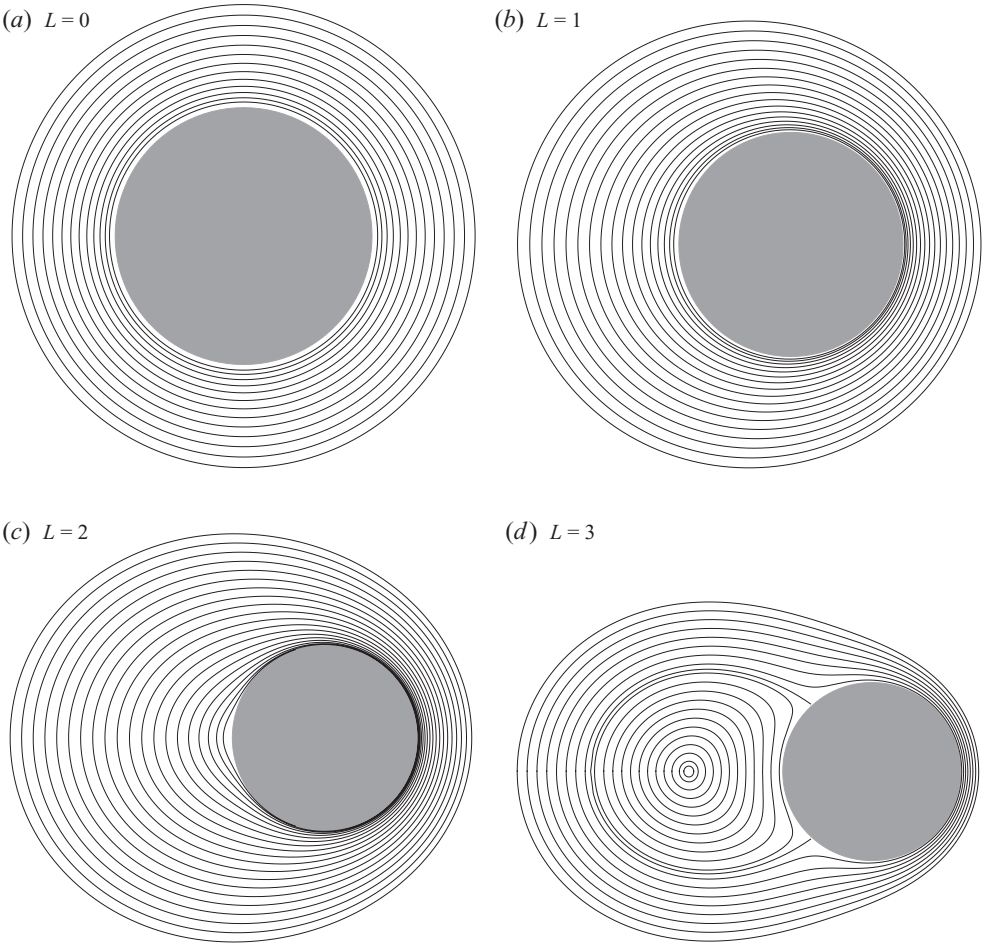


FIGURE 15. Trajectories in the x–y symmetry plane for the case of a rotating background flow.

In parametric formulae, they are

$$x = -\frac{L}{4}\frac{1+s+4s^2}{1+s+s^2}, \tag{5.6}$$

$$z = \pm\sqrt{s^2-x^2} = \pm\frac{\sqrt{16s^2(1+s+s^2)^2+L^2(1+s+4s^2)^2}}{4(1+s+s^2)}, \tag{5.7}$$

where $|s| \geqslant 1$. When $L \leqslant 2$, fixed points in the interior of the fluid connect to the two stagnation points $(-L/2, 0, \sqrt{4-L^2}/2)$ and $(-L/2, 0, \sqrt{4-L^2}/2)$ on the sphere as shown in figures 17(a) and 17(b). Solid dots on the sphere are stagnation points in figure 17. Since fixed points in the fluid are only in the x–z plane, plots in figure 17 are restricted to the x–z plane. The solid curve in figure 17(a) shows the location of fixed points when $L = 0$. Figure 17(b) shows the location of fixed points when $L = 1$. For the degenerate case $L = 2$ shown in figure 17(c), the curve connects to the unique stagnation point $(-1, 0, 0)$ on the sphere. Otherwise, for $L > 2$, as in figure 17(d) ($L = 3$), fixed points are on a curve that is still in the x–z plane but is away from the sphere. All the curves are asymptotic to the rotation axis of the background flow as $|z| \to \infty$. Notice the analogy of these curves of fixed points with those identified off

https://doi.org/10.1017/S0022112010004933 Published online by Cambridge University Press

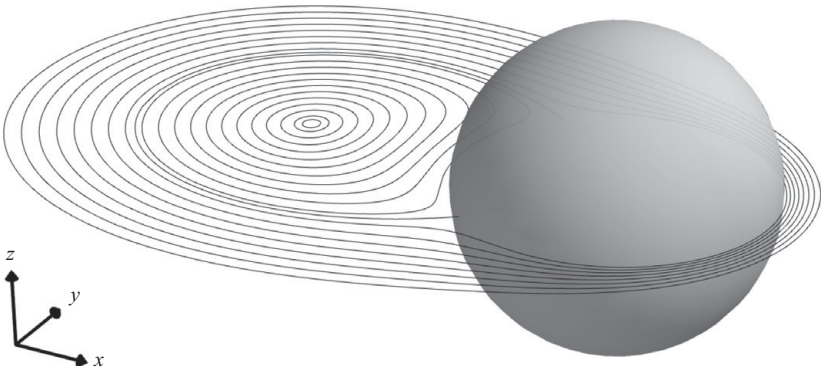


FIGURE 16. 3D view of trajectories in the x–y symmetry plane when $L > 2$.

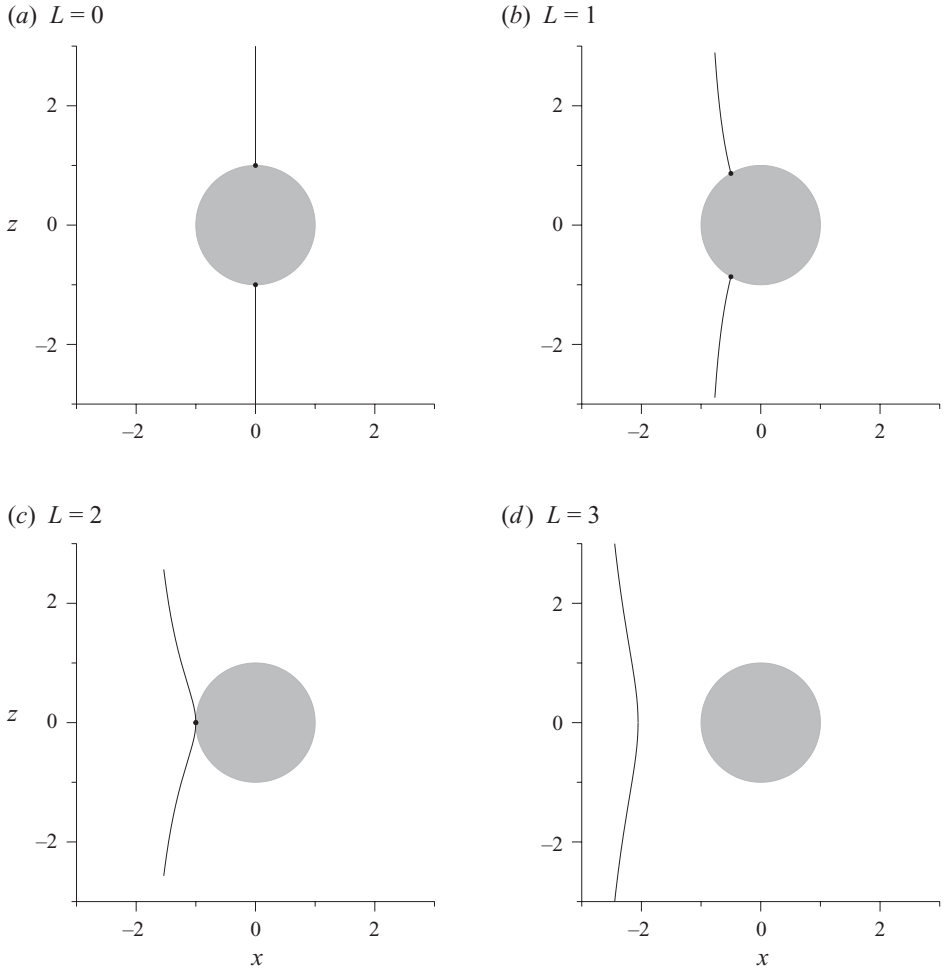


FIGURE 17. (*a–d*) Fixed points in the fluid in the x–z plane when a fixed sphere is embedded in a rotating background flow. L is the distance from the rotation axis of the background flow to the centre of the unit sphere.

https://doi.org/10.1017/S0022112010004933 Published online by Cambridge University Press

the x–z plane by the analysis of the linear planar shear case in §4. The force acting on the fixed sphere is $\boldsymbol{F} = -6\pi\mu L\boldsymbol{e}_y$ and the torque at the origin is $\boldsymbol{T} = -8\pi\mu\boldsymbol{e}_y$ in dimensionless formulae.

5.2. *A self-rotating sphere in the rotating flow*

If the sphere self-rotates in the rotating background flow, imposing the no-slip boundary condition on the rotating sphere requires the velocity on the surface of the sphere to be $\boldsymbol{u}' = -\gamma y\boldsymbol{e}_x + \gamma x\boldsymbol{e}_y$. For the special torque-free case involving a sphere freely self-rotating at the origin, the angular velocity of the self-rotation is set to $\gamma = -1$, as the calculation shows. The exact velocity field is

$$u(x,y,z) = y + \frac{3Lxy}{4(x^2+y^2+z^2)^{3/2}} - \frac{3Lxy}{4(x^2+y^2+z^2)^{5/2}} - \frac{(\gamma+1)y}{(x^2+y^2+z^2)^{3/2}}, \tag{5.8}$$

$$v(x,y,z) = -L - x + \frac{3L}{4\sqrt{x^2+y^2+z^2}} + \frac{4x(\gamma+1)+L(1+3y^2)}{4(x^2+y^2+z^2)^{3/2}} - \frac{3Ly^2}{4(x^2+y^2+z^2)^{5/2}}, \tag{5.9}$$

$$w(x,y,z) = \frac{3Lyz}{4(x^2+y^2+z^2)^{3/2}} - \frac{3Lyz}{4(x^2+y^2+z^2)^{5/2}}. \tag{5.10}$$

And the equation of fluid particles is the following parametric system:

$$x = \frac{r^3}{2L\sqrt{(r-1)^2r^3(1+2r)}}\left\{-\frac{1}{24\sqrt{(1+2r)}}\left[64\gamma\sqrt{3(1+2r)}\operatorname{arctanh}\left(\sqrt{\frac{3r}{1+2r}}\right) + 3(2\sqrt{r}(5+14r+8r^2) + 27\sqrt{2(1+2r)}\log(2\sqrt{r}+\sqrt{2(1+2r)}))\right] - C_1\right\}, \tag{5.11}$$

$$z^2 = \frac{r^3}{C_2(r-1)^2(1+2r)}, \tag{5.12}$$

$$y^2 = r^2 - x^2 - z^2, \tag{5.13}$$

where constants C_1 and C_2 depend on initial values.

Fixed points in the interior of the fluid are

$$\left.\begin{aligned} x &= \frac{L}{4(\gamma+1-r^3)}(4r^3-3r^2-1), \\ z^2 &= r^2 - x^2. \end{aligned}\right\} \tag{5.14}$$

The slope of the fixed-point curve as depicted in figure 18 is $2\gamma/3L$ at $(0,0,1)$, the top of the sphere. For the degenerate cases $L=0$ and $\gamma > -1$, the velocity vanishes not only on the curve prescribed by (5.14) in the x–z plane but also on the shell $x^2+y^2+z^2 = (1+\gamma)^{2/3}$. For the special case $\gamma = 0$ (with the sphere fixed), the location of stagnation points on the sphere depends on L as shown in figure 17. Figure 18 shows the fixed points in the x–z plane for different values of L when the sphere is freely self-rotating in the rotating background flow.

Figure 19 shows the fluid particle trajectories of the freely self-rotating case in the x–y symmetry plane for different values of L. Figure 20 shows trajectories of fluid particles out of the x–y symmetry plane, when $L=4$ and the sphere is freely rotating.

When the orientation of the sphere self-rotation is opposite and equal to that of the background flow, figure 21 shows fixed points in the x–z plane and figure 22 shows

https://doi.org/10.1017/S0022112010004933 Published online by Cambridge University Press

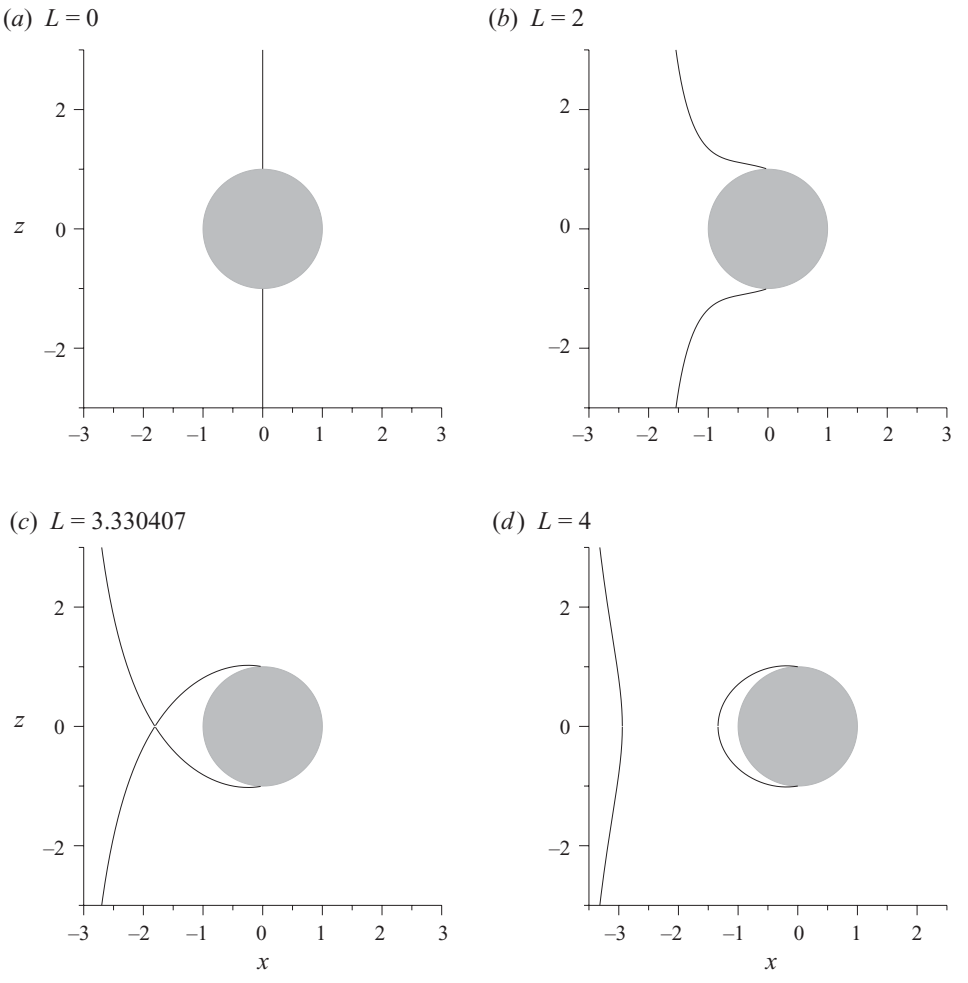


FIGURE 18. (*a–d*) Same as figure 17 but for the case of the sphere freely self-rotating in a rotating background flow.

the trajectories of fluid particles in the x–y symmetry plane with different values of L. Figure 23 shows the structure of the fluid particle trajectories out of the symmetry plane when $L = 3$.

A comparison between these figures shows that the location of the hyperbolic fixed point may be positioned either on the left or on the right side of the sphere, depending upon the parameters.

6. Conclusion and discussion

We have presented an analysis of the fluid particle trajectories for linear shear and rotating flows past a rigid sphere or spheroid in viscosity-dominated regimes. For the symmetric case of a fixed sphere with its centre located on the zero-velocity plane of the linear shear, closed-form expressions provide a complete characterization of the blocking regions. When the sphere centre moves at some distance off this plane, local bifurcations occur in the distance parameter which are analysed analytically, with

https://doi.org/10.1017/S0022112010004933 Published online by Cambridge University Press

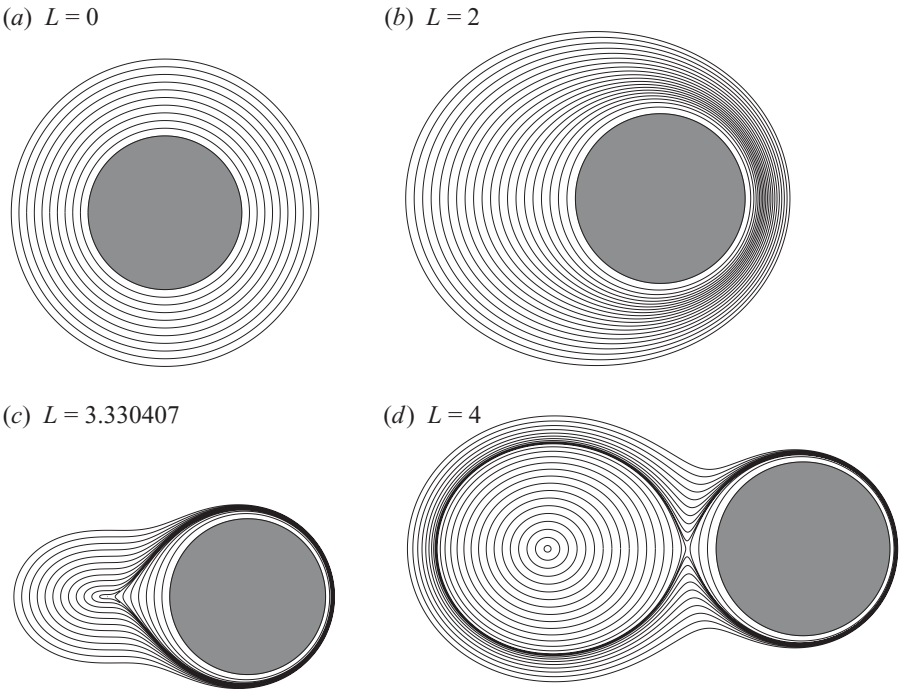


FIGURE 19. (*a–d*) Trajectories in the x–y symmetry plane with a freely-rotating sphere.

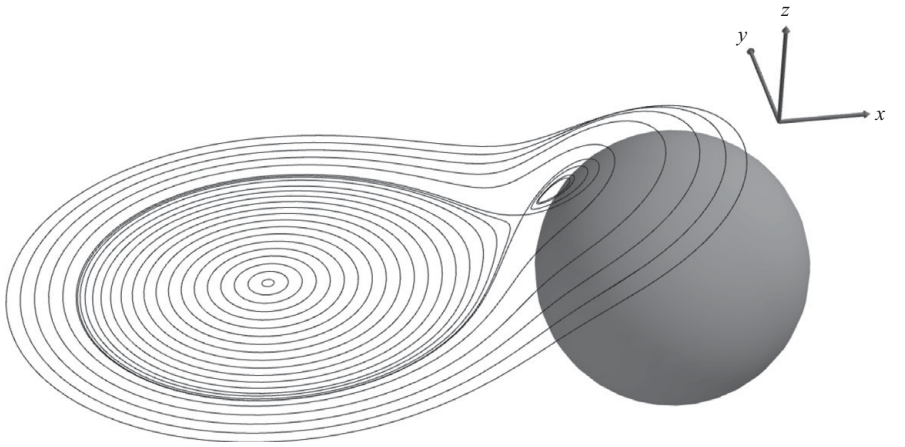


FIGURE 20. Trajectories out of the x–y symmetry plane when the sphere is freely rotating and $L = 4$.

numerical computations showing the persistence and deformations of the blocking regions associated with global bifurcations. For the case involving a background flow past a sphere in rigid-body rotation around a vertical axis, exact expressions for the fluid particle trajectories were presented in all cases. These include the case of a fixed-centre sphere off the axis of the background flow rotation with or without arbitrarily imposed vertical spinning, which may be of importance for studies of

https://doi.org/10.1017/S0022112010004933 Published online by Cambridge University Press

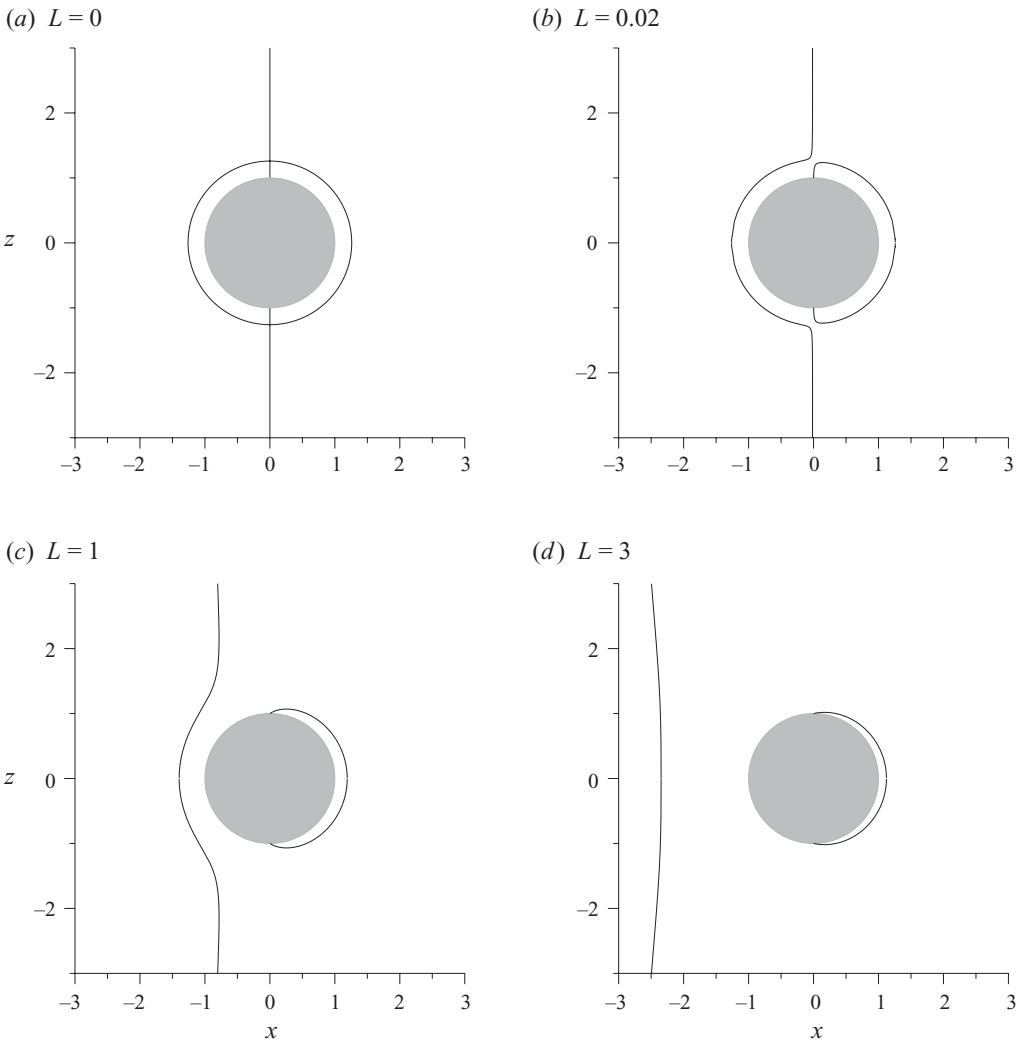


FIGURE 21. (*a–d*) Same as figures 17 and 18 but with a unit sphere self-rotating in an opposite direction with respect to the background flow.

mixing processes. This case is reminiscent of that occurring in the linear background shear flow for large distances off the sphere centre from the zero-velocity plane. Lastly, we have analysed how some of these phenomena are altered when spheres are deformed into prolate spheroids. This introduces an additional orientation to the fluid–body interaction set-up which makes its parametric study much richer. We have concentrated on a subset of this parameter space whence the major spheroid axis lies on the x–z plane. A new behaviour of the fluid flow has emerged in this study, which does not have a counterpart in the spherically symmetric case, namely fluid particle trajectories may be attracted or repelled out of the x–z plane, in positive and negative suction-like patterns. The associated blocking phenomena documented in Appendix A for spheroids are further expected to improve the understanding of the unusual fluid particle trajectories reported by Camassa, Leiterman & McLaughlin (2008) and more

https://doi.org/10.1017/S0022112010004933 Published online by Cambridge University Press

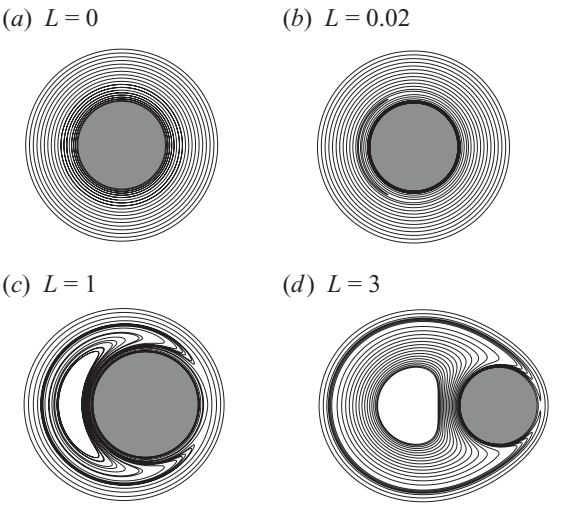


FIGURE 22. (*a–d*) Trajectories in the x–y symmetry plane when the sphere is self-rotating in an opposite direction with respect to the background flow.

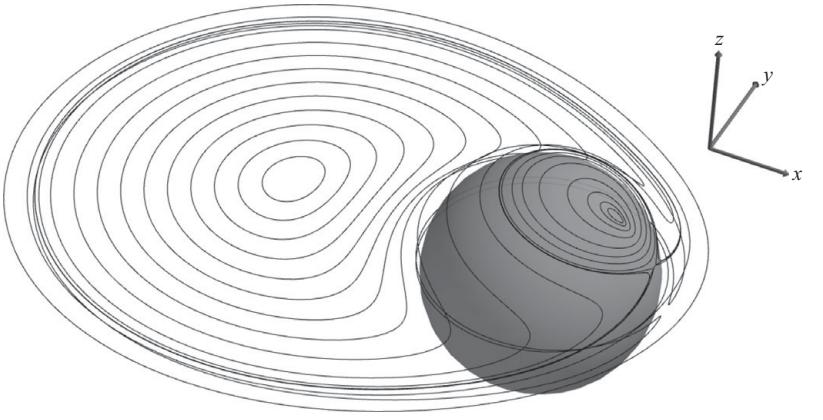


FIGURE 23. Trajectories out of the x–y symmetry plane when the sphere is self-rotating in an opposite direction with respect to the background flow.

generally to understand the flow induced by the motion of cilia in biological systems, such as those examined by Bouzarth *et al.* (2007).

Of particular interest is the behaviour and analysis of the cross-sectional scales of the blocked region. For the case of a fixed sphere centred on the zero-velocity plane, asymptotic estimates were provided which document that this blocking cross-section diverges at large distances from the sphere. We believe that this is the generic behaviour for Stokes' parallel shear flows in exterior domains past rigid bodies. Naturally, this behaviour is somewhat unphysical and should be viewed as yet another form of the Stokes paradox, although in the case of shear emerges in a milder form than e.g. the infinite volume dragged by a uniformly moving sphere. Future studies will investigate the inertial corrections for this unphysical behaviour using matched asymptotics along the lines of the Oseen theory. Such an analysis was

https://doi.org/10.1017/S0022112010004933 Published online by Cambridge University Press

performed by Bretherton (1962) for the special two-dimensional case involving a disk, who showed that logarithmic divergence of the stagnation streamlines bounding the blocked region is suppressed by the inertial terms, making the streamlines settle upon finite height asymptote at infinity. A similar analysis appears to be more involved for the case of a sphere and to our knowledge has never been done. Additional worthy investigations along these lines include assessing behaviours arising from a temporally fluctuating shear flow and/or sphere location as well those associated with more complex rheologies. Finally, the presence of realistic boundary conditions on the exterior fluid domain should be addressed to compare with experiments such as those reported by Poe & Acrivos (1975).

R.C. was partially supported by NSF DMS-0509423 and NSF DMS-0620687. R.M.M. was partially supported by NSF DMS-0308687, RTG NSF DMS-0502266 and NSF NIRT 0507151. L.Z. was partially supported by NSF DMS-0509423 and NSF NIRT 0507151. We thank D. Adalsteinsson for his visualization software DataTank and NSF DMS-SCREMS 04224 for computer support.

Appendix A. Cross-sectional blocking area asymptotics

In this Appendix, we provide the details about the decay rate of the integrand used to compute the cross-sectional area of the blocking region. When the integrand decays fast enough, the integral is convergent, which implies that the cross-sectional area of the blocked region is finite. Otherwise, the integral is divergent and the cross-sectional area is infinite.

The closed integral form trajectory equations (3.32) and (3.33) of the fluid particles are

$$y = y_0 \left(\frac{\left(1-\frac{1}{y_0}\right)^2 \left(\frac{3}{2}\frac{1}{y_0^3}+3\frac{1}{y_0^2}+2\frac{1}{y_0}+1\right)}{\left(1-\frac{1}{r}\right)^2 \left(\frac{3}{2}\frac{1}{r^3}+3\frac{1}{r^2}+2\frac{1}{r}+1\right)} \right)^{1/3}, \tag{A 1}$$

$$z^2 = \frac{1}{\left(1+\frac{3}{2r^5}-\frac{5}{2r^3}\right)^{2/3}} \int_{1/r}^{1/y_0} \frac{(s+1)(1-s)^{1/3}}{\left(\frac{3}{2}s^3+3s^2+2s+1\right)^{1/3}}\,\mathrm{d}s. \tag{A 2}$$

Substituting y and z into the original ODE system used to derive the trajectory equations, we have

$$\begin{aligned}\frac{\mathrm{d}y}{\mathrm{d}r} &= \frac{5\left(\frac{1}{r}+1\right)y}{(1-r)\left(3+6r+4r^2+2r^3\right)} \\ &= \frac{5y_0\left(\frac{1}{r}+1\right)}{(1-r)(3+6r+4r^2+2r^3)} \left(\frac{\left(1-\frac{1}{y_0}\right)^2 \left(\frac{3}{2}\frac{1}{y_0^3}+3\frac{1}{y_0^2}+2\frac{1}{y_0}+1\right)}{\left(1-\frac{1}{r}\right)^2 \left(\frac{3}{2}\frac{1}{r^3}+3\frac{1}{r^2}+2\frac{1}{r}+1\right)} \right)^{1/3},\end{aligned} \tag{A 3}$$

https://doi.org/10.1017/S0022112010004933 Published online by Cambridge University Press

$$\frac{\mathrm{d}z}{\mathrm{d}r} = \frac{(1+r)\left(\frac{5}{r^2}z^2 - 1\right)}{3+3r-2r^2-2r^3-2r^4}\frac{r}{z}$$
$$= \frac{(1+r)r\left(\frac{5}{r^2}\dfrac{1}{\left(\frac{3}{2}\frac{1}{r^5}-\frac{5}{2}\frac{1}{r^3}+1\right)^{2/3}}\displaystyle\int_{1/r}^{1/y_0}\frac{(s+1)(1-s)^{1/3}}{\left(\frac{3}{2}s^3+3s^2+2s+1\right)^{1/3}}\,\mathrm{d}s - 1\right)}{(3+3r-2r^2-2r^3-2r^4)\left\{\dfrac{1}{\left(\frac{3}{2}\frac{1}{r^5}-\frac{5}{2}\frac{1}{r^3}+1\right)^{2/3}}\displaystyle\int_{1/r}^{1/y_0}\frac{(s+1)(1-s)^{1/3}}{\left(\frac{3}{2}s^3+3s^2+2s+1\right)^{1/3}}\,\mathrm{d}s\right\}^{1/2}}. \tag{A 4}$$

All these four equations are in terms of r and y_0.

If $x = x_0$, from $x^2 = r^2 - y^2 - z^2$, we derive the following constraint:

$$\left(1-\frac{5}{2r^3}+\frac{3}{2r^5}\right)^{2/3}\left(r^2-x_0^2\right) = \int_{1/r}^{1/y_0}\frac{(s+1)(1-s)^{1/3}}{\left(\frac{3}{2}s^3+3s^2+2s+1\right)^{1/3}}\,\mathrm{d}s + y_0^2\left(1-\frac{5}{2y_0^3}+\frac{3}{2y_0^5}\right)^{2/3}. \tag{A 5}$$

Taking implicit differentiation, we have

$$\frac{\mathrm{d}r}{\mathrm{d}y_0} = \frac{2y_0^5-y_0^2-1}{y_0^4\left(1-\frac{5}{2r^3}+\frac{3}{2r^5}\right)^{2/3}\left(1-\frac{5}{2y_0^3}+\frac{3}{2y_0^5}\right)^{1/3}}\Bigg/ \left\{\frac{\left(1-\frac{1}{r}\right)\left(1+\frac{1}{r}\right)}{r^2\left(1-\frac{5}{2r^3}+\frac{3}{2r^5}\right)} + \frac{10y_0^2(1+r)}{r(r-1)(3+6r+4r^2+2r^3)}\left(\frac{1+\frac{3}{2y_0^5}-\frac{5}{2y_0^3}}{1-\frac{5}{2r^3}+\frac{3}{2r^5}}\right)^{2/3} + 2r - \frac{5(1-r^2)}{r^6\left(1-\frac{5}{2r^3}+\frac{3}{2r^5}\right)^{5/3}}\int_{1/r}^{1/y_0}\frac{(s+1)(1-s)^{1/3}}{\left(\frac{3}{2}s^3+3s^2+2s+1\right)^{1/3}}\,\mathrm{d}s\right\}. \tag{A 6}$$

Also, from the trajectory equation, we get

$$\frac{\partial y\,(r,\,y_0)}{\partial y_0} = -\frac{\left(y_0^5-1\right)}{y_0^5\left(1-\frac{5}{2r^3}+\frac{3}{2r^5}\right)^{1/3}\left(1-\frac{5}{2y_0^3}+\frac{3}{2y_0^5}\right)^{2/3}}, \tag{A 7}$$

https://doi.org/10.1017/S0022112010004933 Published online by Cambridge University Press

$$\frac{\partial z(r,\,y_0)}{\partial y_0} = -\frac{\left(1-\dfrac{1}{y_0}\right)\left(1+\dfrac{1}{y_0}\right)}{2y_0^2\left(\displaystyle\int_{1/r}^{1/y_0}\frac{(s+1)(1-s)^{1/3}}{\left(\dfrac{3}{2}s^3+3s^2+2s+1\right)^{1/3}}\,\mathrm{d}s\right)^{1/2}} \times\frac{\left(1-\dfrac{5}{2r^3}+\dfrac{3}{2r^5}\right)^{-1/3}}{\left(1+\dfrac{3}{2y_0^5}-\dfrac{5}{2y_0^3}\right)^{1/3}}. \tag{A 8}$$

Now all the components involved in the integral in § 3.5 are in terms of r and y_0.

If $\boldsymbol{a}=(0,\,z)$, then

$$\boldsymbol{a}\cdot\boldsymbol{n} = \frac{z\dfrac{\mathrm{d}y}{\mathrm{d}r}}{\sqrt{\left(\dfrac{\mathrm{d}z}{\mathrm{d}r}\right)^2+\left(\dfrac{\mathrm{d}y}{\mathrm{d}r}\right)^2}}, \quad \mathrm{d}s = \sqrt{\left(\frac{\mathrm{d}z}{\mathrm{d}r}\right)^2+\left(\frac{\mathrm{d}y}{\mathrm{d}r}\right)^2}\,\mathrm{d}r, \tag{A 9}$$

or

$$\boldsymbol{a}\cdot\boldsymbol{n} = \frac{z\dfrac{\mathrm{d}y}{\mathrm{d}y_0}}{\sqrt{\left(\dfrac{\mathrm{d}z}{\mathrm{d}y_0}\right)^2+\left(\dfrac{\mathrm{d}y}{\mathrm{d}y_0}\right)^2}}, \ \mathrm{d}s = \sqrt{\left(\frac{\mathrm{d}z}{\mathrm{d}y_0}\right)^2+\left(\frac{\mathrm{d}y}{\mathrm{d}y_0}\right)^2}\,\mathrm{d}y_0. \tag{A 10}$$

Note the area of the 2D cross-section as I. By the divergence theorem, the area of the 2D cross-section of the blocking region is

$$\begin{aligned}\frac{I}{4} &= \int_\Omega \mathrm{d}A = \int_\Omega \operatorname{div}\boldsymbol{a}\,\mathrm{d}A = \int_{\partial\Omega}\boldsymbol{a}\cdot\boldsymbol{n}\,\mathrm{d}s = \int_1^\infty z\frac{\mathrm{d}y}{\mathrm{d}r}\frac{\mathrm{d}r}{\mathrm{d}y_0}\,\mathrm{d}y_0\\ &= \int_1^\infty z\left(\frac{\partial y}{\partial r}\frac{\partial r}{\partial y_0}+\frac{\partial y}{\partial y_0}\right)\mathrm{d}y_0.\end{aligned} \tag{A 11}$$

We will analyse the integrand involved in the cross-sectional area of the blocking region,

$$z\left(\frac{\partial y}{\partial r}\frac{\partial r}{\partial y_0}+\frac{\partial y}{\partial y_0}\right), \tag{A 12}$$

to study the property of the cross-sectional area of the blocking region.

Substituting (A 1)–(A 8) into the above integrand, we eventually write it as a function of r and y_0,

$$z\left(\frac{\partial y}{\partial r}\frac{\partial r}{\partial y_0}+\frac{\partial y}{\partial y_0}\right) = \frac{1}{\left(1-\dfrac{5}{2r^3}+\dfrac{3}{2r^5}\right)^{2/3}}\left(\int_{1/r}^{1/y_0}\frac{(1+s)(1-s)^{1/3}}{\left(\dfrac{3}{2}s^3+3s^2+2s+1\right)^{1/3}}\,\mathrm{d}s\right)^{1/2}$$

https://doi.org/10.1017/S0022112010004933 Published online by Cambridge University Press

$$\times\left\{\frac{\left(1-\frac{1}{y_0^5}\right)}{\left(1-\frac{5}{2y_0^3}+\frac{3}{2y_0^5}\right)^{2/3}}-\frac{5\left(1+\frac{1}{r}\right)\left(1+\frac{1}{y_0^2}-2y_0^3\right)}{y_0(1-r)(3+6r+4r^2+2r^3)\left(1-\frac{5}{2r^3}+\frac{3}{2r^5}\right)^{2/3}}\right\}\Bigg/$$

$$\left(2r-\frac{102^{2/3}y_0^2\left(1+\frac{3}{2y_0^5}-\frac{5}{2y_0^3}\right)^{2/3}}{r(1-r)(3+6r+4r^2+2r^3)}+\frac{1-\frac{1}{r^2}}{r^2\left(1-\frac{5}{2r^3}+\frac{3}{2r^5}\right)}\right.$$

$$\left.-\frac{5(1-r^2)}{r^6\left(1-\frac{5}{2r^3}+\frac{3}{2r^5}\right)^{5/3}}\int_{1/r}^{1/y_0}\frac{(s+1)(1-s)^{1/3}}{\left(\frac{3}{2}s^3+3s^2+2s+1\right)^{1/3}}\,\mathrm{d}s\right)\Bigg\}. \tag{A 13}$$

If x_0 is a fixed finite number, from the constraint (A 5), we get the asymptotic solution $r\sim\sqrt{y_0^2+x_0^2}$. Substitute this solution into the above equation. The integrand

$$z\left(\frac{\partial y}{\partial r}\frac{\partial r}{\partial y_0}+\frac{\partial y}{\partial y_0}\right)\sim\frac{x_0}{\sqrt{2}y_0^{3/2}}\quad\text{as}\quad y_0\to\infty. \tag{A 14}$$

At a finite distance $|x_0|$ from the sphere, the cross-sectional area of the blocking region depends on x_0 and is finite.

If the cross-section is taken at infinite $x_0=\infty$, then

$$y\sim y_0\left(\left(1-\frac{1}{y_0}\right)^2\left(1+\frac{3}{2y_0^3}+\frac{3}{y_0^2}+\frac{2}{y_0}\right)\right)^{1/3}, \tag{A 15}$$

$$z^2\sim\int_0^{1/y_0}\frac{(s+1)(1-s)^{1/3}}{\left(\frac{3}{2}s^3+3s^2+2s+1\right)^{1/3}}\,\mathrm{d}s. \tag{A 16}$$

The cross-sectional area I is computed as

$$\frac{I}{4}=\int_\Omega \mathrm{d}A=\int_\Omega \mathrm{div}\,\boldsymbol{a}\,\mathrm{d}A=\int_{\partial\Omega}\boldsymbol{a}\cdot\boldsymbol{n}\,\mathrm{d}s=\int_1^\infty z\frac{\mathrm{d}y}{\mathrm{d}y_0}\,\mathrm{d}y_0. \tag{A 17}$$

The integrand decays as

$$z\frac{\mathrm{d}y}{\mathrm{d}y_0}\sim\left(\int_0^{1/y_0}\frac{(s+1)(1-s)^{1/3}}{\left(\frac{3}{2}s^3+3s^2+2s+1\right)^{1/3}}\,\mathrm{d}s\right)^{1/2}\left(\frac{2^{2/3}\left(y_0^5-1\right)\left(\frac{y_0^5}{3-5y_0^2+2y_0^5}\right)^{2/3}}{y_0^5}\right)$$

$$\sim\frac{1}{\sqrt{y_0}}+\frac{5}{3}\left(\frac{1}{y_0}\right)^{7/2}\quad\text{as}\quad y_0\to\infty. \tag{A 18}$$

With such a decay rate, the integral is divergent. Far enough from the sphere, the cross-sectional area is infinite.

To understand the growth of the area, we assume $x_0=y_0^\epsilon$ $(\epsilon>0)$, then from the constraint (A 5) we get the asymptotic solution $r\sim\sqrt{y_0^2+y_0^{2\epsilon}}$. Substituting this

https://doi.org/10.1017/S0022112010004933 Published online by Cambridge University Press

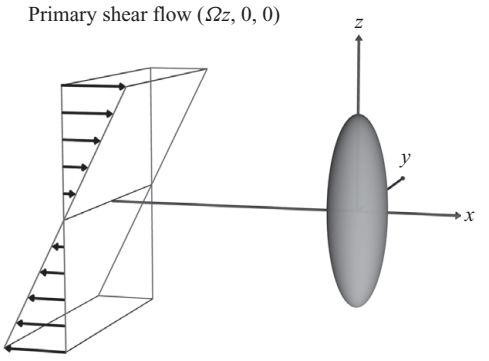


FIGURE 24. A linear shear flow passes a fixed prolate spheroid. The major axis is perpendicular to the direction of the shear flow (an upright spheroid).

solution into the integrand (A 13) and computing the asymptotic as $y_0 \to \infty$, we have the following.

(i) When $0 < \epsilon < 1$, as $y_0 \to \infty$, the leading order of the integrand (A 13) is

$$z\left(\frac{\partial y}{\partial r}\frac{\partial r}{\partial y_0} + \frac{\partial y}{\partial y_0}\right) \sim -\frac{y_0^{-(3/2)+\epsilon}}{\sqrt{2}} \quad \text{as} \quad y_0 \to \infty. \tag{A 19}$$

As $y_0 \to \infty$, the integrand decays like $y_0^{-(3/2)+\epsilon}$. Consequently, when $0 < \epsilon < 1/2$, the integral is convergent. When $\epsilon \geqslant 1/2$, the integral is divergent.

(ii) When $\epsilon \geqslant 1$, as $y_0 \to \infty$, the leading order of the integrand (A 13) is

$$z\left(\frac{\partial y}{\partial r}\frac{\partial r}{\partial y_0} + \frac{\partial y}{\partial y_0}\right) \sim -\frac{3}{2\sqrt{y_0}} \quad \text{as} \quad y_0 \to \infty. \tag{A 20}$$

In this case, the cross-sectional area of the blocking region is infinite.

Appendix B. Shear flow past a spheroid

In this Appendix, we focus on the flow structure and blocking phenomena for a prolate spheroid embedded in a linear shear flow. With respect to the spherical case, the spheroid orientation relative to the background shear enriches the phenomena, some of which will be examined here. The literature on this set-up has concentrated mostly on forces and torques (Blaser 2002), while some experimental investigations of three-dimensional separation structures for flows past spheroids can be found in the high Reynolds regime (Wang *et al.* 1990).

First, we report results about the shear flow $\Omega z \boldsymbol{e}_x$ when the spheroid sits with its centre on the zero-velocity plane and its major axis upright (as shown in figure 24),

$$\frac{x^2 + y^2}{b^2} + \frac{z^2}{a^2} = 1, \tag{B 1}$$

where $a > b$ are the major and minor semi-axes, respectively, and the half focal length c and the eccentricity e are defined as $c = (a^2 - b^2)^{1/2} = e\,a$. From Chwang & Wu (1975), the exact velocity field in this case is

$$\boldsymbol{u}(x) = \Omega z \boldsymbol{e}_x - \int_{-c}^{c} (c^2 - \xi^2)(\alpha \boldsymbol{U}_{SS}(\boldsymbol{x} - \boldsymbol{\xi}; \boldsymbol{e}_z, \boldsymbol{e}_x) + \gamma \boldsymbol{U}_R(\boldsymbol{x} - \boldsymbol{\xi}; \boldsymbol{e}_y))\,\mathrm{d}\xi$$
$$- \beta \int_{-c}^{c} (c^2 - \xi^2)^2 \partial_z \boldsymbol{U}_D(\boldsymbol{x} - \boldsymbol{\xi}; \boldsymbol{e}_x)\,\mathrm{d}\xi, \tag{B 2}$$

https://doi.org/10.1017/S0022112010004933 Published online by Cambridge University Press

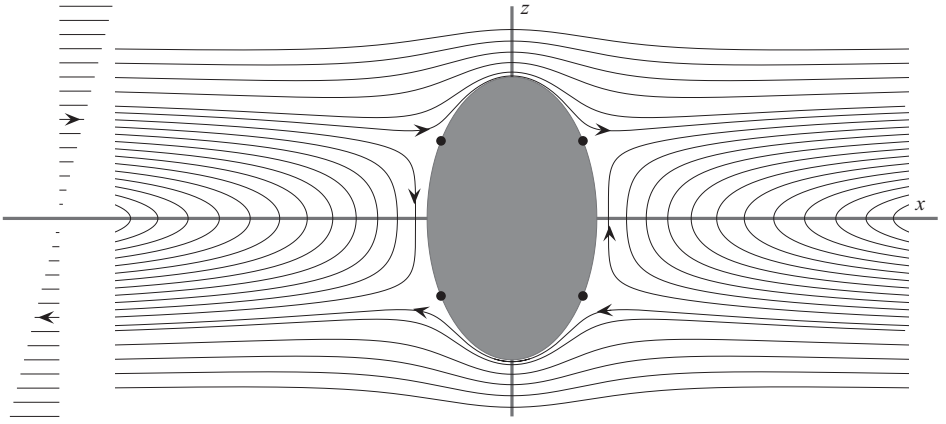


FIGURE 25. Streamlines in the $y=0$ symmetry plane for a linear shear past a fixed upright spheroid. The four points mark the stagnation points on the spheroid.

where $\boldsymbol{U}_{SS}$, $\boldsymbol{U}_R$ and $\boldsymbol{U}_D$ are the fundamental singularities of stresslet, rotlet and doublelet, located at $\boldsymbol{\xi}$,

$$U_{SS}(\boldsymbol{x}-\boldsymbol{\xi};\boldsymbol{e}_z,\boldsymbol{e}_x)=\frac{3((\boldsymbol{x}-\boldsymbol{\xi})\cdot\boldsymbol{e}_z)((\boldsymbol{x}-\boldsymbol{\xi})\cdot\boldsymbol{e}_x)}{R^5}(\boldsymbol{x}-\boldsymbol{\xi}), \tag{B 3}$$

$$U_R(\boldsymbol{x}-\boldsymbol{\xi},\boldsymbol{e}_y)=\frac{(\boldsymbol{x}-\boldsymbol{\xi})\times\boldsymbol{e}_y}{R^3}, \tag{B 4}$$

$$U_D(\boldsymbol{x}-\boldsymbol{\xi},\boldsymbol{e}_x)=-\frac{\boldsymbol{e}_x}{R^3}+\frac{3(\boldsymbol{x}-\boldsymbol{\xi})\cdot\boldsymbol{e}_x}{R^5}(\boldsymbol{x}-\boldsymbol{\xi}), \tag{B 5}$$

with $R=\sqrt{x^2+y^2+(z-\xi)^2}$, and $\boldsymbol{\xi}=\xi\boldsymbol{e}_z$. Here, α, β and γ are known constants,

$$\alpha=\beta\frac{4e^2}{1-e^2}=\gamma e^2\frac{-2e+(1-e^2)L_e}{2e(2e^2-3)+3(1-e^2)L_e},\quad \gamma=\frac{\Omega}{-2e+(1+e^2)L_e}, \tag{B 6}$$

and $L_e=\log((1+e)/(1-e))$. Numerical results show the existence of blocked regions in the flow, as shown in figure 25, where the streamlines are plotted in the $y=0$ symmetry plane.

B.1. *Stagnation points on the spheroid*

From the velocity field (B 2), we find the stagnation points on the spheroid. As before for the spherical case, we first rewrite the velocity field in prolate spherical coordinates

$$\left.\begin{aligned} x&=a\,e\sinh(\mu)\sin(\nu)\cos(\phi),\\ y&=a\,e\sinh(\mu)\sin(\nu)\sin(\phi),\\ z&=a\,e\cosh(\mu)\cos(\nu),\end{aligned}\right\} \tag{B 7}$$

where $\operatorname{arccosh}(1/e)\leqslant\mu\leqslant\infty$, $0\leqslant\nu\leqslant\pi$ and $-\pi\leqslant\phi<\pi$ (more details about the explicit velocity field are provided by Zhao 2010). Next, we rescale the time $\tau=(\mu-\operatorname{arccosh}(1/e))\,t$ and expand the velocity field near the no-slip boundary of the spheroid where $\mu=\operatorname{arccosh}(1/e)$, ignoring higher-order terms of order $(\mu-\operatorname{arccosh}(1/e))^2$. The linearized ODE system for the trajectory of fluid particle

https://doi.org/10.1017/S0022112010004933 Published online by Cambridge University Press

near the surface of the spheroid reduces to

$$\left.\begin{aligned}\frac{\mathrm{d}\mu}{\mathrm{d}\tau} &= 0,\\ \frac{\mathrm{d}\nu}{\mathrm{d}\tau} &= 4\,\omega e^3\,\frac{k(e)}{d(e)}\frac{\cos(\phi)}{e^2+e^2\cos(2\nu)-2},\\ \frac{\mathrm{d}\phi}{\mathrm{d}\tau} &= 4\,\omega e^3\,\frac{[2e(3-e^2)+(e^4+2e^2-3)L_e]}{d(e)}\frac{\cot(\nu)\sin(\phi)}{1-e^2},\end{aligned}\right\} \tag{B 8}$$

where

$$d(e) \equiv 12e^2 - 8e^4 + 4e(e^4+e^2-3)L_e - 3(e^4-1)L_e^2 \tag{B 9}$$

and

$$k(e) \equiv 2e(6-e^2) + (e^4+3e^2-6)L_e + e^2\cos(2\nu)((1+e^2)L_e - 2e). \tag{B 10}$$

The conditions for stagnation points on the boundary,

$$\frac{\mathrm{d}\mu}{\mathrm{d}\tau} = 0, \quad \frac{\mathrm{d}\nu}{\mathrm{d}\tau} = 0 \quad \text{and} \quad \frac{\mathrm{d}\phi}{\mathrm{d}\tau} = 0, \tag{B 11}$$

define six stagnation points on the upright prolate spheroid in the prolate spherical coordinates

$$a\left(\operatorname{arccosh}(1/e), \frac{\pi}{2}, \frac{\pi}{2}\right), \quad a\left(\operatorname{arccosh}(1/e), \frac{3\pi}{2}, \frac{\pi}{2}\right), \tag{B 12}$$

$$a\left(\operatorname{arccosh}(1/e), 0, \arccos\left(\pm\left(\frac{6e-(3-e^2)L_e}{2e^3-e^2(1+e^2)L_e}\right)^{1/2}\right)\right) \tag{B 13}$$

and

$$a\left(\operatorname{arccosh}(1/e), \pi, \arccos\left(\pm\left(\frac{6e-(3-e^2)L_e}{2e^3-e^2(1+e^2)L_e}\right)^{1/2}\right)\right). \tag{B 14}$$

In the original rectangular coordinates, the latter stagnation points lie in the $y=0$ symmetry plane

$$a\left(\pm\sqrt{1-e^2}\left(1-\frac{6e-(3-e^2)L_e}{2e^3-e^2(1+e^2)L_e}\right)^{1/2}, 0, \pm\left(\frac{6e-(3-e^2)L_e}{2e^3-e^2(1+e^2)L_e}\right)^{1/2}\right), \tag{B 15}$$

while the other two are on the y-axis at $(0, \pm a\sqrt{1-e^2}, 0)$.

The location of the stagnation points in the $y=0$ symmetry plane migrates towards the spheroid 'tips' with increasing eccentricity e at fixed a. The four points merge into two at the tips in the 'needle' limit of eccentricity $e \to 1$, while for the opposite limit of a sphere ($e \to 0$) we retrieve the previous result (3.25). Just like for the spherical case, the zero-velocity plane of the background shear flow collapses to just the y-axis for the upright spheroid whose centre is on this plane.

B.2. *Characterization of stagnation streamlines on the surface of the spheroid*

As for the case of the sphere, the rescaled velocity field provides an imprint of the particle trajectory pattern just off the spheroid surface which mathematically reduces to heteroclinic connections between the stagnation points (see figure 26).

https://doi.org/10.1017/S0022112010004933 Published online by Cambridge University Press

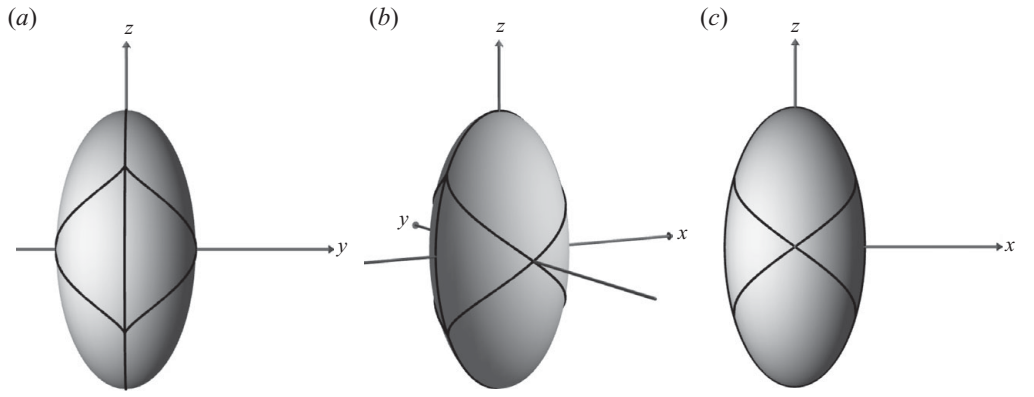


FIGURE 26. (*a–c*) 'Footprint' of stagnation surfaces on the spheroid surface from different viewpoints.

From the rescaled velocity field ODE (B 8), we get

$$\frac{\mathrm{d}\nu}{\mathrm{d}\phi} = \frac{(1-e^2)k(e)\cot(\phi)\tan(\nu)}{(e^2\cos(2\nu)+e^2-2)[2e(3-e^2)+(e^4+2e^2-3)L_e]}, \tag{B 16}$$

whose solution is

$$\sin(\phi)\sin(\nu) = C\,(k(e))^{p(e)}, \tag{B 17}$$

where the constant C is determined by the initial conditions, and the constant $p(e)$ is

$$p(e) \equiv \frac{2e+(e^2-1)L_e}{(1-e^2)((1+e^2)L_e-2e)}. \tag{B 18}$$

Substituting the stagnation points yields the trajectories

$$x^2 = (1-e^2)(a^2-z^2) - y^2 = a^2(1-e^2)\sin^2(\nu) - y^2, \tag{B 19}$$

$$y = a\sqrt{1-e^2}\sin(\nu)\sin(\phi) = a\sqrt{1-e^2}\,C(k(e))^{p(e)}, \tag{B 20}$$

$$z = a\cos(\nu), \tag{B 21}$$

in the first octant (x, y, z positive), which can be extended by the symmetry of the flow to the whole space.

B.3. *Linear shear flow past a tilted spheroid*

When the major axis of the spheroid is tilted with an angle κ, defined as the angle between the positive z-axis and the major axis of the spheroid in the x–z plane (see figures 27*a* and 28*a*), the $y=0$ plane is still a symmetry plane of the flow but the up-down symmetry of the fluid–body set-up is broken. The tilted prolate spheroid is

$$\frac{(x\cos(\kappa)-z\sin(\kappa))^2+y^2}{b^2} + \frac{(x\sin(\kappa)+z\cos(\kappa))^2}{a^2} = 1 \quad (a>b>0). \tag{B 22}$$

(The previous case is recovered for $\kappa=0$.)

The solution of Stokes equations for this tilted case can be efficiently obtained in the body frame from the general theory of Chwang & Wu (1975) and Jeffery (1922). In this frame, the spheroid's major axis is on the x-axis, and the background flow can be decomposed into two shear flows $x\boldsymbol{e}_y$ and $y\boldsymbol{e}_x$ and an elongational flow $x\boldsymbol{e}_x - y\boldsymbol{e}_y$. For each of these shear flows, the velocity field is given by changing coordinates

https://doi.org/10.1017/S0022112010004933 Published online by Cambridge University Press

(*a*) Configuration (*b*) Streamlines

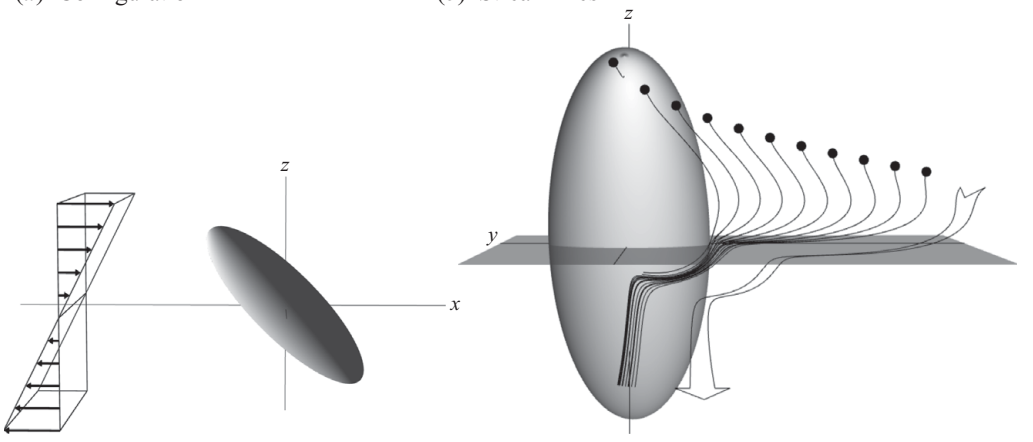


FIGURE 27. (*a–b*) Blocked streamlines near the separation surface in the $y<0$ half-space when the spheroid is tilted towards the shear with $\kappa=-\pi/4$. Particles initially distributed on a curve within the blocked region move downwards while being attracted towards the body as indicated by the perspective arrow on the right.

of (B 2) for the first one, and

$$\boldsymbol{u}(x)=y\boldsymbol{e}_x+\int_{-c}^{c}(c^2-\xi^2)(\alpha_3\boldsymbol{U}_{SS}(\boldsymbol{x}-\boldsymbol{\xi};\boldsymbol{e}_x,\boldsymbol{e}_y)+\gamma_3\boldsymbol{U}_R(\boldsymbol{x}-\boldsymbol{\xi};\boldsymbol{e}_z))\,\mathrm{d}\xi + \beta_3\int_{-c}^{c}(c^2-\xi^2)^2\partial_y\boldsymbol{U}_{\mathrm{D}}(\boldsymbol{x}-\boldsymbol{\xi};\boldsymbol{e}_x)\,\mathrm{d}\xi, \quad \text{(B 23)}$$

for the second, respectively. Here

$$\gamma_3=\frac{1-e^2}{-2e+(1+e^2)L_e},\quad \beta_3=\frac{(1-e^2)(L_e-2e)}{4e(2e^2-3)+6(1-e^2)L_e}\gamma_3 \quad\text{and}\quad \alpha_3=\frac{4e^2}{1-e^2}\beta_3. \quad \text{(B 24)}$$

For the elongational flow $\Omega x\boldsymbol{e}_x-\Omega y\boldsymbol{e}_y$, the velocity field is (Jeffery 1922)

$$\begin{aligned}
u&=x\{\Omega+\beta'(W-V)-2(\alpha+2\beta)A\}\\
&\quad-\frac{2xP^2}{(a^2+\lambda)^{3/2}(b^2+\lambda)^3}[\{W-2(a^2+\lambda)A+2(b^2+\lambda)B\}y^2\\
&\quad-\{V-2(b^2+\lambda)C+2(a^2+\lambda)A\}z^2], \quad \text{(B 25)}\\
v&=y\{-\Omega+\alpha'U-\beta'W-2(\alpha+2\beta)B\}\\
&\quad-\frac{2yP^2}{(a^2+\lambda)^{1/2}(b^2+\lambda)^2}[\{U-2(b^2+\lambda)B+2(b^2+\lambda)C\}z^2/(b^2+\lambda)^2\\
&\quad-\{W-2(a^2+\lambda)A+2(b^2+\lambda)B\}x^2/(a^2+\lambda)^2], \quad \text{(B 26)}\\
w&=z\{\beta'V-\alpha'U-2(\alpha+2\beta)C\}\\
&\quad-\frac{2zP^2}{(a^2+\lambda)^{1/2}(b^2+\lambda)^2}[\{V-2(b^2+\lambda)C+2(a^2+\lambda)A\}x^2/(a^2+\lambda)^2\\
&\quad-\{U-2(b^2+\lambda)B+2(b^2+\lambda)C\}y^2/(b^2+\lambda)^2], \quad \text{(B 27)}
\end{aligned}$$

https://doi.org/10.1017/S0022112010004933 Published online by Cambridge University Press

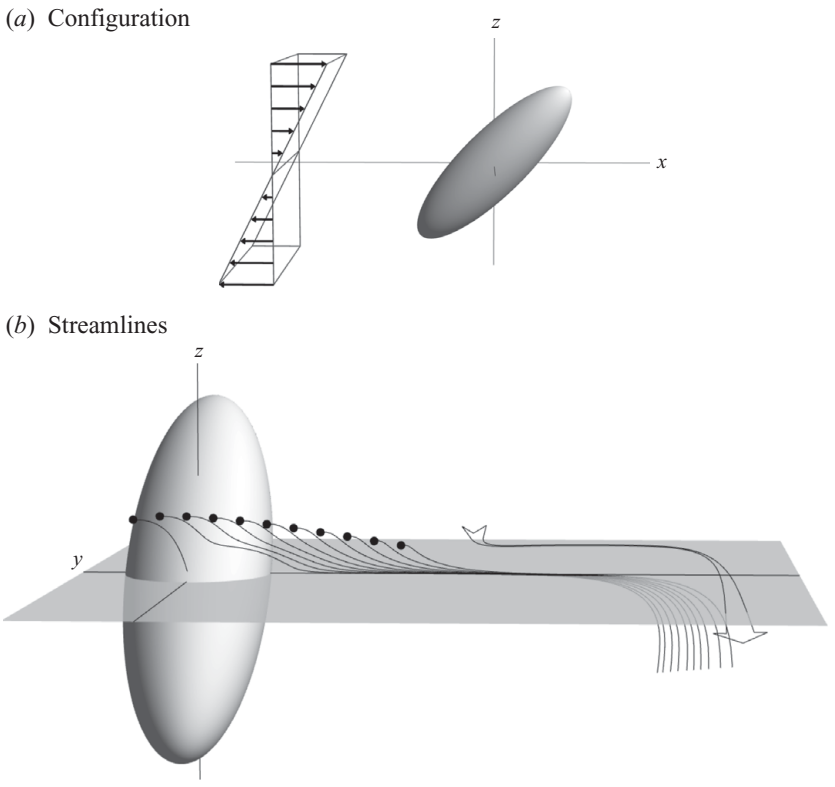


FIGURE 28. (*a–b*) Similar to figure 27, blocked streamlines near the separation surface in the $y<0$ half-space, when the spheroid is tilted along the shear with $\kappa=\pi/4$.

where

$$\lambda=\frac{1}{2}(x^2+y^2+z^2-a^2-b^2 + \sqrt{(x^2+y^2+z^2-a^2-b^2)^2+4\{a^2(y^2+z^2-b^2)+b^2x^2\}}), \tag{B 28}$$

$$P^2=\left(\frac{x^2}{(a^2+\lambda^2)^2}+\frac{y^2+z^2}{(b^2+\lambda)^2}\right)^{-1}, \tag{B 29}$$

and

$$\alpha=\int_\lambda^\infty \frac{1}{(a^2+\lambda)^{3/2}(b^2+\lambda)}\,\mathrm{d}\lambda, \quad \beta=\int_\lambda^\infty \frac{1}{\sqrt{a^2+\lambda}(b^2+\lambda)^2}\,\mathrm{d}\lambda, \tag{B 30}$$

$$\alpha'=\int_\lambda^\infty \frac{1}{\sqrt{a^2+\lambda}(b^2+\lambda)^3}\,\mathrm{d}\lambda, \quad \beta'=\int_\lambda^\infty \frac{1}{(a^2+\lambda)^{3/2}(b^2+\lambda)^2}\,\mathrm{d}\lambda, \tag{B 31}$$

$$\alpha''=\beta-b^2\alpha', \qquad \beta''=\alpha-b^2\beta'. \tag{B 32}$$

The constants A–W are

$$A=\frac{\Omega}{6\beta_0''}, \quad B=\Omega\frac{-2\beta_0''-\alpha_0''}{6\beta_0''(\beta_0''+2\alpha_0'')}, \quad C=\Omega\frac{-\alpha_0''+\beta_0''}{6\beta_0''(\beta_0''+2\alpha_0'')}, \tag{B 33}$$

https://doi.org/10.1017/S0022112010004933 Published online by Cambridge University Press

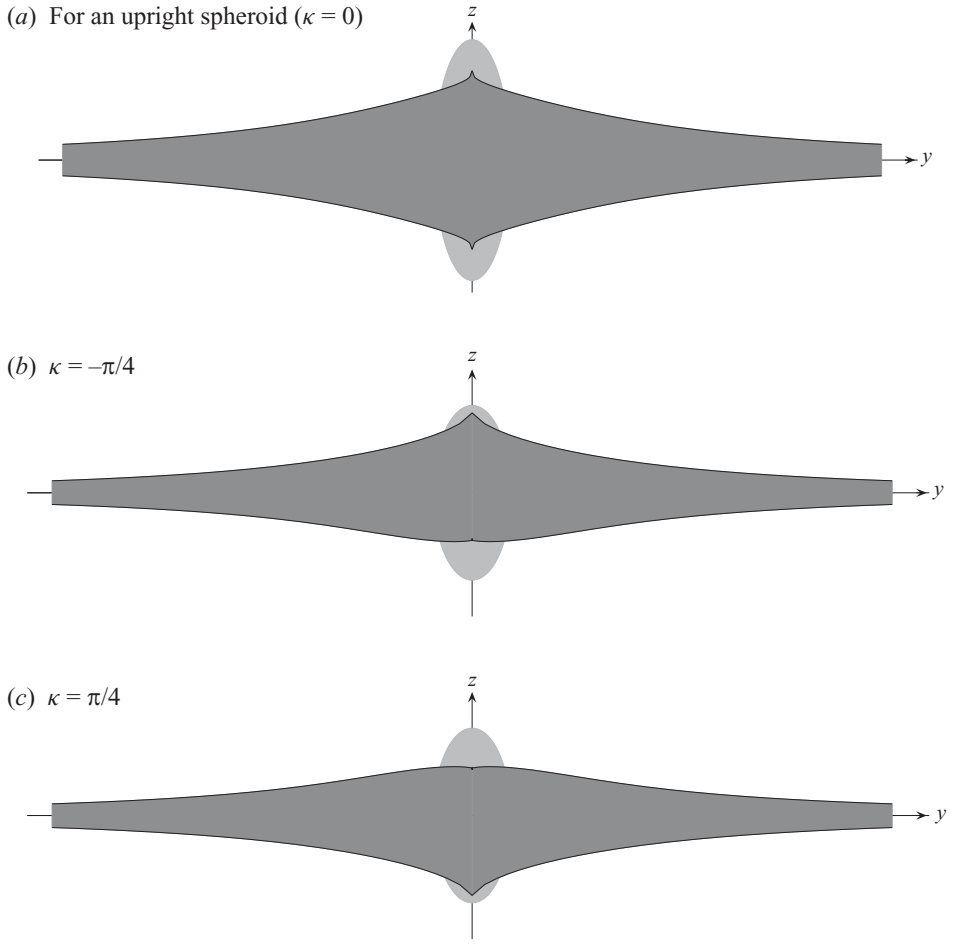


FIGURE 29. Cross-section of the blocked region at $x = -5$ fixed.

$$U = -\frac{\Omega b^2}{2\alpha_0'' + \beta_0''}, \quad V = \frac{\Omega b^2(\beta_0'' - \alpha_0'')}{3\beta_0''(\beta_0'' + 2\alpha_0'')} - \frac{\Omega a^2}{3\beta_0''}, \quad W = \frac{\Omega a^2}{3\beta_0''} + \frac{\Omega b^2(2\beta_0'' + \alpha_0'')}{3\beta_0''(\beta_0'' + 2\alpha_0'')}, \tag{B 34}$$

where

$$\alpha_0'' = \frac{3 - e^2}{4a^3e^4(1 - e^2)} - \frac{(e^2 + 3)L_e}{8a^3e^5} \tag{B 35}$$

and

$$\beta_0'' = \frac{-6e + (3 - e^2)L_e}{2a^3e^5} \tag{B 36}$$

are α'' and β'' evaluated at $\lambda = 0$, respectively. (More details about the velocity field in the original laboratory frame are provided by Zhao 2010.)

As for the other cases we have discussed, six stagnation points on the tilted spheroid are obtained by rescaling the velocity field in prolate spherical coordinates and linearizing it near the surface. Two of the stagnation points are located at

https://doi.org/10.1017/S0022112010004933 Published online by Cambridge University Press

$(0, \pm b, 0)$, while the location of the other four are defined by the solutions of the following equation in prolate spheroid coordinates:

$$\frac{\cos(2\kappa)\cos(2\nu)}{3(1-e^2)L_e + 2e(2e^2-3)} - \frac{\{22e^3 - 18e + (9 - 14e^2 + 5e^4)L_e\}\sin(2\kappa)\sin(2\nu)}{2\sqrt{1-e^2}(6e + (e^2-3)L_e)(2e(5e^2-3) + 3(e^2-1)^2 L_e)} + \frac{12e - 8e^3 - 6(1-e^2)L_e + (6e + (e^2-3)L_e)e^2\cos(2\kappa)}{e^2(3(1-e^2)L_e + 2e(2e^2-3))((1+e^2)L_e - 2e)} = 0. \tag{B 37}$$

This equation yields two values of the angle ν between 0 and π, corresponding to two stagnation points on the spheroid in the $y=0$ symmetry plane. In the original rectangular coordinates, where the spheroid is tilted in the shear flow, these two stagnation points are defined by substituting such solutions ν into

$$\begin{pmatrix} x_s \\ y_s \\ z_s \end{pmatrix} = a \begin{pmatrix} -\sin(\kappa)\cos(\nu) - \sqrt{1-e^2}\cos(\kappa)\sin(\nu) \\ 0 \\ \cos(\kappa)\cos(\nu) - \sqrt{1-e^2}\sin(\kappa)\sin(\nu) \end{pmatrix}. \tag{B 38}$$

Using the specular symmetry of the set-up with respect to the origin in the $y=0$ plane locates the other two stagnation points.

Figures 27 and 28 are plots of numerically evaluated streamlines from the above exact velocity field in the laboratory frame which illustrates the main features of the flow. When the spheroid is tilted in the x–z plane, the portion of the y-axis in the fluid turns into a stagnation streamline, as opposed to a line of fixed points for the upright case, i.e. points on the y-axis move in the y-direction. However, the y-axis keeps its feature of being the intersection of separation surfaces bounding the blocked region of fluid. For a given spheroid, the maximum speed on the y-axis streamline is achieved at a certain finite location on this axis for the tilt corresponding to the angle $\kappa = \pm\pi/4$. The speed along the y-axis is zero on the body and at infinity.

(i) When the spheroid is tilted towards the background linear shear ($\kappa < 0$), on the y-axis, the flow pushes the fluid particles towards to the spheroid. Figure 27(a) shows the configuration of the linear shear and the tilted spheroid with $\kappa = -\pi/4$, and figure 27(b) shows the positive suction of the fluid particles when the particle trajectories are close to the separation surface.

(ii) When the spheroid is tilted along the background linear shear ($\kappa > 0$), on the y-axis, the flow pushes the fluid particles away from the spheroid. The configuration of the linear shear and the tilted spheroid with $\kappa = \pi/4$ is shown in figure 28(a), and the negative suction of the fluid particles is illustrated with the blocked fluid particle trajectories close to the separation surface in figure 28(b).

For the cross-section of the blocked region, when the spheroid is upright or horizontal, i.e. when its major axis is aligned along the z- or x-axis, respectively, the up-down symmetry (reflections with respect to the x–y plane) of the set-up is preserved; in this case, the cross-section is symmetric, as shown in figure 29(a). This is similar to the spherical case in figure 6, but notice that corners develop on the bounding surfaces along the $y=0$ plane. The cross-section height is a decreasing function of y. When the spheroid is tilted in the x–z plane, the up-down symmetry of the cross-section is also broken: when the spheroid is tilted against the background

https://doi.org/10.1017/S0022112010004933 Published online by Cambridge University Press

stream ($\kappa < 0$), both boundaries of the cross-section are concave upward near $y = 0$; when the spheroid is tilted along the background linear shear ($\kappa > 0$), both boundaries of the cross-section are concave downward near $y = 0$. Figures 29(b) and 29(c) are cross-sections of the blocked region with $\kappa = -\pi/4$ and $\kappa = \pi/4$, respectively.

Near the corners, the concavity of the boundaries of the blocked region is determined by the spheroid eccentricity e and the tilt angle κ. From the local analysis near the stagnation points (B 38) in the symmetry plane, the eigenvectors of the matrix of the linearized velocity in the general body frame, where the spheroid is along the x-axis, are $(0, 0, a)$ and $a(0, \sqrt{1-e^2}\sin(\nu), \cos(\nu))$. When these two vectors are perpendicular to each other, i.e. the eccentricity e and the tilt angle $\pm\kappa$ satisfy

$$\frac{12e - 8e^3 - 6(1-e^2)L_e + (6e + (e^2-3)L_e)e^2\cos(2\kappa)}{e^2(3(1-e^2)L_e + 2e(2e^2-3))((1+e^2)L_e - 2e)} - \frac{\cos(2\kappa)}{3(1-e^2)L_e + 2e(2e^2-3)} = 0, \quad \text{(B 39)}$$

the concavity of the blocked region changes.

REFERENCES

Blaser, S. 2002 Forces on the surface of small ellipsoidal particles immersed in a linear flow field. *Chem. Engng Sci.* **57**, 515–526.

Bouzarth, E. L., Brooks, A., Camassa, R., Jing, H., Leiterman, T. J., Mclaughlin, R. M., Superfine, R., Toledo, J. & Vicci, L. 2007 Epicyclic orbits in a viscous fluid about a precessing rod: theory and experiments at the micro- and macro-scales. *Phys. Rev.* E **76** (1), 016313, 1–5.

Bretherton, F. P. 1962 Slow viscous motion round a cylinder in a simple shear. *J. Fluid Mech.* **12**, 591–613.

Camassa, R., Leiterman, T. J. & McLaughlin, R. M. 2008 Trajectory and flow properties for a rod spinning in a viscous fluid. Part 1. An exact solution. *J. Fluid Mech.* **612**, 153–200.

Chwang, A. T. & Wu, T. Y. 1975 Hydromechanics of low-Reynolds-number flow. Part 2. Singularity method for Stokes flows. *J. Fluid Mech.* **67**, 787–815.

Cox, R. G., Zia, Y. Z. & Mason, S. G. 1968 Particle motion in sheared suspensions. XXV. Streamline around cylinders and spheres. *J. Colloid Interface Sci.* **27**, 7–18.

Feke, D. L. & Schowalter, W. R. 1983 The effect of Brownian diffusion on shear-induced coagulation of colloidal dispersions. *J. Fluid Mech.* **133**, 17–35.

Jeffrey, D. J. & Sherwood, J. D. 1980 Streamline patterns and eddies in low-Reynolds-number flow. *J. Fluid Mech.* **96**, 315–334.

Jeffery, G. B. 1922 The motion of ellipsoidal particles immersed in a viscous fluid. *Proc. R. Soc. Lond.* A **102**, 161–179.

Kim, S. & Karrila, S. J. 2005 *Microhydrodynamics: Principles and Selected Applications*. Dover.

Kossack, C. A. & Acrivos, A. 1974 Steady simple shear flow past a circular cylinder at moderate Reynolds numbers: a numerical solution. *J. Fluid Mech.* **66**, 353–376.

Leal, L. G. 2007 *Advanced Transport Phenomena: Fluid Mechanics and Convective Transport Processes*. Cambridge University Press.

Ma, T. & Wang, S. 2001 A generalized Poincaré–Hopf index formula and its applications to 2-D incompressible flows. *Nonlinear Anal. Real World Appl.* **1**, 467–482.

Mikulencak, D. R. & Morris, J. F. 2004 Stationary shear flow around fixed and free bodies at finite Reynolds number. *J. Fluid Mech.* **520**, 215–242.

Poe, G. G. & Acrivos, A. 1975 Closed streamline flows past rotating single cylinders and spheres: inertia effects. *J. Fluid Mech.* **72**, 605–623.

Pozrikidis, C. 1997 *Introduction to Theoretical and Computational Fluid Dynamics*. Oxford University Press.

https://doi.org/10.1017/S0022112010004933 Published online by Cambridge University Press

Robertson, C. R. & Acrivos, A. 1970 Low Reynolds number shear flow past a rotating circular cylinder. Part 1. Momentum transfer. *J. Fluid Mech.* **40**, 685–704.

Saffman, P. G. 1965 Lift on a small sphere in a slow shear flow. *J. Fluid Mech.* **22**, 385–400.

Spielman, L. A. 1977 Particle capture from low-speed laminar flows. *Annu. Rev. Fluid Mech.* **9**, 297–319.

Wang, K. C., Zhou, H. C., Hu, C. H. & Harrington, S. 1990 Three-dimensional separated flow structure over prolate spheroids. *Proc. R. Soc. Lond.* A **421**, 73–91.

Zhao, L. 2010 Fluid–structure interaction in viscous dominated flows. PhD thesis, University of North Carolina at Chapel Hill.

https://doi.org/10.1017/S0022112010004933 Published online by Cambridge University Press